



NOAA Atlas NESDIS 52

WORLD OCEAN ATLAS 2001 VOLUME 4: Nutrients

Margarita E. Conkright
Hernan E. Garcia
Todd D. O'Brien
Ricardo A. Locarnini
Timothy P. Boyer
Cathy Stephens
John I. Antonov

Editor: Sydney Levitus

National Oceanographic Data Center
Ocean Climate Laboratory

Silver Spring, MD
May 2002

U.S. DEPARTMENT OF COMMERCE
Donald L. Evans, Secretary

National Oceanic and Atmospheric Administration
Vice Admiral Conrad C. Lautenbacher, Jr. USN (Ret.)
Under Secretary of Commerce for Oceans and Atmosphere

National Environmental Satellite, Data, and Information Service
Gregory W. Withee, Assistant Administrator

National Oceanographic Data Center

Additional copies of this publication, as well as information about NODC data holdings, and services, are available on request directly from NODC. NODC information and data are also available over the Internet through the NODC World Wide site.

National Oceanographic Data Center
User Services Team
NOAA/NESDIS E/OC1
SSM3, 4th Floor
1315 East-West Highway
Silver Spring, MD 20910-3282

Telephone: (301)713-3277

Fax: (301)713-3302

E-mail: services@nodc.noaa.gov

NODC World Wide Web site: <http://www.nodc.noaa.gov/OC5>

For updates on the data, documentation and additional information about WOA01 please refer to:

<http://www.nodc.noaa.gov>

click on: Ocean Climate Laboratory
click on: Products

This publication should be cited as:

Conkright, M.E., H.E. Garcia, T.D. O'Brien, R.A. Locarnini, T.P. Boyer, C. Stephens, J.I. Antonov ,
2002: *World Ocean Atlas 2001, Volume 4: Nutrients*. Ed. S. Levitus, NOAA Atlas NESDIS 52,
U.S. Government Printing Office, Wash., D.C., 392 pp.

Contents

Preface	xiii
Acknowledgments	xiv
Abstract	1
1. Introduction	1
2. Data and data distribution	1
2.1 Data sources	1
2.2 Data quality control	2
2.2a Duplicate elimination	2
2.2b Range checks and gradient checks	2
2.2c Statistical checks	2
2.2d Subjective flagging of data	3
2.2e Representativeness of the data	3
3. Data processing procedures	3
3.1 Vertical interpolation to standard levels	3
3.2 Methods of analysis	4
3.2a Overview	4
3.2b Derivation of Barnes (1964) weight function	5
3.2c Derivation of Barnes (1964) response function	6
3.2d Choice of response function	6
3.2e First-guess field determination	6
3.3 Choice of objective analysis procedures	7
3.4 Choice of spatial grid	7
4. Results	8
4.1 Computation of annual and seasonal fields	8
4.2 Explanation of standard level figures	8
4.3 Standard level analyses	8
4.4 Contents of the <i>World Ocean Atlas 2001</i> CD-ROM	8
5. Summary	9
6. Future work	9
7. References	10
8. Appendix A: Annual distribution by one-degree squares of the number of phosphate observations and the mean at selected standard levels for the climatological annual compositing period	21
9. Appendix B: Seasonal distribution of phosphate observations, seasonal mean, and seasonal minus annual means at selected standard levels	45
10. Appendix C: Monthly distribution of phosphate observations, mean, and monthly minus annual means at selected standard levels	85
11. Appendix D: Annual distribution by one-degree squares of the number of nitrate observations and the mean at selected standard levels for the climatological annual compositing period	145
12. Appendix E: Seasonal distribution of nitrate observations, seasonal mean, and seasonal minus annual means at selected standard levels	169

13. Appendix F:	Monthly distribution of nitrate observations, mean, and monthly minus annual means at selected standard levels	209
14. Appendix G:	Annual distribution by one-degree squares of the number of silicate observations and the mean at selected standard levels for the climatological annual compositing period	269
15. Appendix H:	Seasonal distribution of silicate observations, seasonal mean, and seasonal minus annual means at selected standard levels	293
16. Appendix I:	Monthly distribution of silicate observations, mean, and monthly minus annual means at selected standard levels	333

List of Tables

Table 1	Acceptable distances (m) for defining interior and exterior values used in the Reiniger-Ross scheme for interpolating observed level data to standard levels.
Table 2	Response function of the objective analysis scheme as a function of wavelength for WOA01 and earlier analyses.
Table 3	Basins defined for objective analysis and the shallowest standard depth level for which each basin is defined.

List of Figures

Fig. 1a.	Annual phosphate standard deviation (μM) at 500 meters depth by one-degree squares.
Fig. 1b.	Annual nitrate standard error of the mean (μM) at 500 meters depth by one-degree squares.
Fig. 2.	Response function of the WOA01, WOA98, WOA94 and Levitus (1982) objective analysis schemes.
Fig 3	Scheme used in computing annual, seasonal, and monthly objectively analyzed means for a variable.
Fig. 4.	Annual observed one-degree square silicate mean value minus objectively analyzed annual mean silicate values (μM) at 500 meters depth by one-degree squares.

APPENDIX A

Fig. A1.	Annual distribution of phosphate observations at the surface.
Fig. A2.	Annual distribution of phosphate observations at 50 m depth.
Fig. A3.	Annual distribution of phosphate observations at 75 m depth.
Fig. A4.	Annual distribution of phosphate observations at 100 m depth.
Fig. A5.	Annual distribution of phosphate observations at 150 m depth.
Fig. A6.	Annual distribution of phosphate observations at 200 m depth.
Fig. A7.	Annual distribution of phosphate observations at 250 m depth.
Fig. A8.	Annual distribution of phosphate observations at 400 m depth.
Fig. A9.	Annual distribution of phosphate observations at 500 m depth.
Fig. A10.	Annual distribution of phosphate observations at 700 m depth.
Fig. A11.	Annual distribution of phosphate observations at 1000 m depth.
Fig. A12.	Annual distribution of phosphate observations at 1500 m depth.
Fig. A13.	Annual distribution of phosphate observations at 2000 m depth.
Fig. A14.	Annual distribution of phosphate observations at 2500 m depth.
Fig. A15.	Annual distribution of phosphate observations at 3000 m depth.
Fig. A16.	Annual distribution of phosphate observations at 4000 m depth.
Fig. A17.	Annual mean phosphate (μM) at the surface.
Fig. A18.	Annual mean phosphate (μM) at 50 m depth.
Fig. A19.	Annual mean phosphate (μM) at 75 m depth.
Fig. A20.	Annual mean phosphate (μM) at 100 m depth.
Fig. A21.	Annual mean phosphate (μM) at 150 m depth.
Fig. A22.	Annual mean phosphate (μM) at 200 m depth.
Fig. A23.	Annual mean phosphate (μM) at 250 m depth.

- Fig. A24. Annual mean phosphate (μM) at 400 m depth.
- Fig. A25. Annual mean phosphate (μM) at 500 m depth.
- Fig. A26. Annual mean phosphate (μM) at 700 m depth.
- Fig. A27. Annual mean phosphate (μM) at 1000 m depth.
- Fig. A28. Annual mean phosphate (μM) at 1500 m depth.
- Fig. A29. Annual mean phosphate (μM) at 2000 m depth.
- Fig. A30. Annual mean phosphate (μM) at 2500 m depth.
- Fig. A31. Annual mean phosphate (μM) at 3000 m depth.
- Fig. A32. Annual mean phosphate (μM) at 4000 m depth.

APPENDIX B

- Fig. B1. Winter (Jan.-Mar.) distribution of phosphate observations at the surface.
- Fig. B2. Winter (Jan.-Mar.) distribution of phosphate observations at 75 m depth.
- Fig. B3. Winter (Jan.-Mar.) distribution of phosphate observations at 150 m depth.
- Fig. B4. Winter (Jan.-Mar.) distribution of phosphate observations at 250 m depth.
- Fig. B5. Spring (Apr.-Jun.) distribution of phosphate observations at the surface.
- Fig. B6. Spring (Apr.-Jun.) distribution of phosphate observations at 75 m depth.
- Fig. B7. Spring (Apr.-Jun.) distribution of phosphate observations at 150 m depth.
- Fig. B8. Spring (Apr.-Jun.) distribution of phosphate observations at 250 m depth.
- Fig. B9. Summer (Jul.-Sep.) distribution of phosphate observations at the surface.
- Fig. B10. Summer (Jul.-Sep.) distribution of phosphate observations at 75 m depth.
- Fig. B11. Summer (Jul.-Sep.) distribution of phosphate observations at 150 m depth.
- Fig. B12. Summer (Jul.-Sep.) distribution of phosphate observations at 250 m depth.
- Fig. B13. Fall (Oct.-Dec.) distribution of phosphate observations at the surface.
- Fig. B14. Fall (Oct.-Dec.) distribution of phosphate observations at 75 m depth.
- Fig. B15. Fall (Oct.-Dec.) distribution of phosphate observations at 150 m depth.
- Fig. B16. Fall (Oct.-Dec.) distribution of phosphate observations at 250 m depth.

- Fig. B17. Winter (Jan.-Mar.) mean phosphate (μM) at the surface.
- Fig. B18. Winter (Jan.-Mar.) minus annual mean phosphate (μM) at the surface.
- Fig. B19. Winter (Jan.-Mar.) mean phosphate (μM) at 75 m depth.
- Fig. B20. Winter (Jan.-Mar.) minus annual mean phosphate (μM) at 75 m depth.
- Fig. B21. Winter (Jan.-Mar.) mean phosphate (μM) at 150 m depth.
- Fig. B22. Winter (Jan.-Mar.) minus annual mean phosphate (μM) at 150 m depth.
- Fig. B23. Winter (Jan.-Mar.) mean phosphate (μM) at 250 m depth.
- Fig. B24. Winter (Jan.-Mar.) minus annual mean phosphate (μM) at 250 m depth.
- Fig. B25. Spring (Apr.-Jun.) mean phosphate (μM) at the surface.
- Fig. B26. Spring (Apr.-Jun.) minus annual mean phosphate (μM) at the surface.
- Fig. B27. Spring (Apr.-Jun.) mean phosphate (μM) at 75 m depth.
- Fig. B28. Spring (Apr.-Jun.) minus annual mean phosphate (μM) at 75 m depth.
- Fig. B29. Spring (Apr.-Jun.) mean phosphate (μM) at 150 m depth.
- Fig. B30. Spring (Apr.-Jun.) minus annual mean phosphate (μM) at 150 m depth.
- Fig. B31. Spring (Apr.-Jun.) mean phosphate (μM) at 250 m depth.
- Fig. B32. Spring (Apr.-Jun.) minus annual mean phosphate (μM) at 250 m depth.
- Fig. B33. Summer (Jul.-Sep.) mean phosphate (μM) at the surface.
- Fig. B34. Summer (Jul.-Sep.) mean minus annual phosphate (μM) at the surface.
- Fig. B35. Summer (Jul.-Sep.) mean phosphate (μM) at 75 m depth.
- Fig. B36. Summer (Jul.-Sep.) mean minus annual phosphate (μM) at 75 m depth.
- Fig. B37. Summer (Jul.-Sep.) mean phosphate (μM) at 150 m depth.
- Fig. B38. Summer (Jul.-Sep.) mean minus annual phosphate (μM) at 150 m depth.
- Fig. B39. Summer (Jul.-Sep.) mean phosphate (μM) at 250 m depth.
- Fig. B40. Summer (Jul.-Sep.) mean minus annual phosphate (μM) at 250 m depth.
- Fig. B41. Fall (Oct.-Dec.) mean phosphate (μM) at the surface.
- Fig. B42. Fall (Oct.-Dec.) mean minus annual phosphate (μM) at the surface.
- Fig. B43. Fall (Oct.-Dec.) mean phosphate (μM) at 75 m depth.
- Fig. B44. Fall (Oct.-Dec.) mean minus annual phosphate (μM) at 75 m depth.
- Fig. B45. Fall (Oct.-Dec.) mean phosphate (μM) at 150 m depth.
- Fig. B46. Fall (Oct.-Dec.) mean minus annual phosphate (μM) at 150 m depth.

- Fig. B47 Fall (Oct.-Dec.) mean phosphate (μM) at 250 m depth.
 Fig. B48 Fall (Oct.-Dec.) mean minus annual phosphate (μM) at 250 m depth.

APPENDIX C

- Fig. C1 January distribution of phosphate observations at the surface.
 Fig. C2 January distribution of phosphate observations at 75 m depth.
 Fig. C3 February distribution of phosphate observations at the surface.
 Fig. C4 February distribution of phosphate observations at 75 m depth.
 Fig. C5 March distribution of phosphate observations at the surface.
 Fig. C6 March distribution of phosphate observations at 75 m depth.
 Fig. C7 April distribution of phosphate observations at the surface.
 Fig. C8 April distribution of phosphate observations at 75 m depth.
 Fig. C9 May distribution of phosphate observations at the surface.
 Fig. C10 May distribution of phosphate observations at 75 m depth.
 Fig. C11 June distribution of phosphate observations at the surface.
 Fig. C12 June distribution of phosphate observations at 75 m depth.
 Fig. C13 July distribution of phosphate observations at the surface.
 Fig. C14 July distribution of phosphate observations at 75 m depth.
 Fig. C15 August distribution of phosphate observations at the surface.
 Fig. C16 August distribution of phosphate observations at 75 m depth.
 Fig. C17 September distribution of phosphate observations at the surface.
 Fig. C18 September distribution of phosphate observations at 75 m depth.
 Fig. C19 October distribution of phosphate observations at the surface.
 Fig. C20 October distribution of phosphate observations at 75 m depth.
 Fig. C21 November distribution of phosphate observations at the surface.
 Fig. C22 November distribution of phosphate observations at 75 m depth.
 Fig. C23 December distribution of phosphate observations at the surface.
 Fig. C24 December distribution of phosphate observations at 75 m depth.
- Fig. C25 January mean phosphate (μM) at the surface.
 Fig. C26 January mean minus annual phosphate (μM) at the surface.
 Fig. C27 January mean phosphate (μM) at 75 m depth.
 Fig. C28 January mean minus annual phosphate (μM) at 75 m depth.
 Fig. C29 February mean phosphate (μM) at the surface.
 Fig. C30 February mean minus annual phosphate (μM) at the surface.
 Fig. C31 February mean phosphate (μM) at 75 m depth.
 Fig. C32 February mean minus annual phosphate (μM) at 75 m depth.
 Fig. C33 March mean phosphate (μM) at the surface.
 Fig. C34 March mean minus annual phosphate (μM) at the surface.
 Fig. C35 March mean phosphate (μM) at 75 m depth.
 Fig. C36 March mean minus annual phosphate (μM) at 75 m depth.
 Fig. C37 April mean phosphate (μM) at the surface.
 Fig. C38 April mean minus annual phosphate (μM) at the surface.
 Fig. C39 April mean phosphate (μM) at 75 m depth.
 Fig. C40 April mean minus annual phosphate (μM) at 75 m depth.
 Fig. C41 May mean phosphate (μM) at the surface.
 Fig. C42 May mean minus annual phosphate (μM) at the surface.
 Fig. C43 May mean phosphate (μM) at 75 m depth.
 Fig. C44 May mean minus annual phosphate (μM) at 75 m depth.
 Fig. C45 June mean phosphate (μM) at the surface.
 Fig. C46 June mean minus annual phosphate (μM) at the surface.
 Fig. C47 June mean phosphate (μM) at 75 m depth.
 Fig. C48 June mean minus annual phosphate (μM) at 75 m depth.
 Fig. C49 July mean phosphate (μM) at the surface.
 Fig. C50 July mean minus annual phosphate (μM) at the surface.
 Fig. C51 July mean phosphate (μM) at 75 m depth.
 Fig. C52 July mean minus annual phosphate (μM) at 75 m depth.

Fig. C53 August mean phosphate (μM) at the surface.
 Fig. C54 August mean minus annual phosphate (μM) at the surface.
 Fig. C55 August mean phosphate (μM) at 75 m depth.
 Fig. C56 August mean minus annual phosphate (μM) at 75 m depth.
 Fig. C57 September mean phosphate (μM) at the surface.
 Fig. C58 September mean minus annual phosphate (μM) at the surface.
 Fig. C59 September mean phosphate (μM) at 75 m depth.
 Fig. C60 September mean minus annual phosphate (μM) at 75 m depth.
 Fig. C61 October mean phosphate (μM) at the surface.
 Fig. C62 October mean minus annual phosphate (μM) at the surface.
 Fig. C63 October mean phosphate (μM) at 75 m depth.
 Fig. C64 October mean minus annual phosphate (μM) at 75 m depth.
 Fig. C65 November mean phosphate (μM) at the surface.
 Fig. C66 November mean minus annual phosphate (μM) at the surface.
 Fig. C67 November mean phosphate (μM) at 75 m depth.
 Fig. C68 November mean minus annual phosphate (μM) at 75 m depth.
 Fig. C69 December mean phosphate (μM) at the surface.
 Fig. C70 December mean minus annual phosphate (μM) at the surface.
 Fig. C71 December mean phosphate (μM) at 75 m depth.
 Fig. C72 December mean minus annual phosphate (μM) at 75 m depth.

APPENDIX D

Fig. D1. Annual distribution of nitrate observations at the surface.
 Fig. D2. Annual distribution of nitrate observations at 50 m depth.
 Fig. D3. Annual distribution of nitrate observations at 75 m depth.
 Fig. D4. Annual distribution of nitrate observations at 100 m depth.
 Fig. D5. Annual distribution of nitrate observations at 150 m depth.
 Fig. D6. Annual distribution of nitrate observations at 200 m depth.
 Fig. D7. Annual distribution of nitrate observations at 250 m depth.
 Fig. D8. Annual distribution of nitrate observations at 400 m depth.
 Fig. D9. Annual distribution of nitrate observations at 500 m depth.
 Fig. D10. Annual distribution of nitrate observations at 700 m depth.
 Fig. D11. Annual distribution of nitrate observations at 1000 m depth.
 Fig. D12. Annual distribution of nitrate observations at 1500 m depth.
 Fig. D13. Annual distribution of nitrate observations at 2000 m depth.
 Fig. D14. Annual distribution of nitrate observations at 2500 m depth.
 Fig. D15. Annual distribution of nitrate observations at 3000 m depth.
 Fig. D16. Annual distribution of nitrate observations at 4000 m depth.

Fig. D17. Annual mean nitrate (μM) at the surface.
 Fig. D18. Annual mean nitrate (μM) at 50 m depth.
 Fig. D19. Annual mean nitrate (μM) at 75 m depth.
 Fig. D20. Annual mean nitrate (μM) at 100 m depth.
 Fig. D21. Annual mean nitrate (μM) at 150 m depth.
 Fig. D22. Annual mean nitrate (μM) at 200 m depth.
 Fig. D23. Annual mean nitrate (μM) at 250 m depth.
 Fig. D24. Annual mean nitrate (μM) at 400 m depth.
 Fig. D25. Annual mean nitrate (μM) at 500 m depth.
 Fig. D26. Annual mean nitrate (μM) at 700 m depth.
 Fig. D27. Annual mean nitrate (μM) at 1000 m depth.
 Fig. D28. Annual mean nitrate (μM) at 1500 m depth.
 Fig. D29. Annual mean nitrate (μM) at 2000 m depth.
 Fig. D30. Annual mean nitrate (μM) at 2500 m depth.
 Fig. D31. Annual mean nitrate (μM) at 3000 m depth.
 Fig. D32. Annual mean nitrate (μM) at 4000 m depth.

APPENDIX E

- Fig. E1. Winter (Jan.-Mar.) distribution of nitrate observations at the surface.
- Fig. E2. Winter (Jan.-Mar.) distribution of nitrate observations at 75 m depth.
- Fig. E3. Winter (Jan.-Mar.) distribution of nitrate observations at 150 m depth.
- Fig. E4. Winter (Jan.-Mar.) distribution of nitrate observations at 250 m depth.
- Fig. E5. Spring (Apr.-Jun.) distribution of nitrate observations at the surface.
- Fig. E6. Spring (Apr.-Jun.) distribution of nitrate observations at 75 m depth.
- Fig. E7. Spring (Apr.-Jun.) distribution of nitrate observations at 150 m depth.
- Fig. E8. Spring (Apr.-Jun.) distribution of nitrate observations at 250 m depth.
- Fig. E9. Summer (Jul.-Sep.) distribution of nitrate observations at the surface.
- Fig. E10. Summer (Jul.-Sep.) distribution of nitrate observations at 75 m depth.
- Fig. E11. Summer (Jul.-Sep.) distribution of nitrate observations at 150 m depth.
- Fig. E12. Summer (Jul.-Sep.) distribution of nitrate observations at 250 m depth.
- Fig. E13. Fall (Oct.-Dec.) distribution of nitrate observations at the surface.
- Fig. E14. Fall (Oct.-Dec.) distribution of nitrate observations at 75 m depth.
- Fig. E15. Fall (Oct.-Dec.) distribution of nitrate observations at 150 m depth.
- Fig. E16. Fall (Oct.-Dec.) distribution of nitrate observations at 250 m depth.

- Fig. E17. Winter (Jan.-Mar.) mean nitrate (μM) at the surface.
- Fig. E18. Winter (Jan.-Mar.) minus annual mean nitrate (μM) at the surface.
- Fig. E19. Winter (Jan.-Mar.) mean nitrate (μM) at 75 m depth.
- Fig. E20. Winter (Jan.-Mar.) minus annual mean nitrate (μM) at 75 m depth.
- Fig. E21. Winter (Jan.-Mar.) mean nitrate (μM) at 150 m depth.
- Fig. E22. Winter (Jan.-Mar.) minus annual mean nitrate (μM) at 150 m depth.
- Fig. E23. Winter (Jan.-Mar.) mean nitrate (μM) at 250 m depth.
- Fig. E24. Winter (Jan.-Mar.) minus annual mean nitrate (μM) at 250 m depth.
- Fig. E25. Spring (Apr.-Jun.) mean nitrate (μM) at the surface.
- Fig. E26. Spring (Apr.-Jun.) minus annual mean nitrate (μM) at the surface.
- Fig. E27. Spring (Apr.-Jun.) mean nitrate (μM) at 75 m depth.
- Fig. E28. Spring (Apr.-Jun.) minus annual mean nitrate (μM) at 75 m depth.
- Fig. E29. Spring (Apr.-Jun.) mean nitrate (μM) at 150 m depth.
- Fig. E30. Spring (Apr.-Jun.) minus annual mean nitrate (μM) at 150 m depth.
- Fig. E31. Spring (Apr.-Jun.) mean nitrate (μM) at 250 m depth.
- Fig. E32. Spring (Apr.-Jun.) minus annual mean nitrate (μM) at 250 m depth.
- Fig. E33. Summer (Jul.-Sep.) mean nitrate (μM) at the surface.
- Fig. E34. Summer (Jul.-Sep.) mean minus annual nitrate (μM) at the surface.
- Fig. E35. Summer (Jul.-Sep.) mean nitrate (μM) at 75 m depth.
- Fig. E36. Summer (Jul.-Sep.) mean minus annual nitrate (μM) at 75 m depth.
- Fig. E37. Summer (Jul.-Sep.) mean nitrate (μM) at 150 m depth.
- Fig. E38. Summer (Jul.-Sep.) mean minus annual nitrate (μM) at 150 m depth.
- Fig. E39. Summer (Jul.-Sep.) mean nitrate (μM) at 250 m depth.
- Fig. E40. Summer (Jul.-Sep.) mean minus annual nitrate (μM) at 250 m depth.
- Fig. E41. Fall (Oct.-Dec.) mean nitrate (μM) at the surface.
- Fig. E42. Fall (Oct.-Dec.) mean minus annual nitrate (μM) at the surface.
- Fig. E43. Fall (Oct.-Dec.) mean nitrate (μM) at 75 m depth.
- Fig. E44. Fall (Oct.-Dec.) mean minus annual nitrate (μM) at 75 m depth.
- Fig. E45. Fall (Oct.-Dec.) mean nitrate (μM) at 150 m depth.
- Fig. E46. Fall (Oct.-Dec.) mean minus annual nitrate (μM) at 150 m depth.
- Fig. E47. Fall (Oct.-Dec.) mean nitrate (μM) at 250 m depth.
- Fig. E48. Fall (Oct.-Dec.) mean minus annual nitrate (μM) at 250 m depth.

APPENDIX F

- Fig. F1. January distribution of nitrate observations at the surface.
- Fig. F2. January distribution of nitrate observations at 75 m depth.
- Fig. F3. February distribution of nitrate observations at the surface.
- Fig. F4. February distribution of nitrate observations at 75 m depth.

Fig. F5 March distribution of nitrate observations at the surface.
 Fig. F6 March distribution of nitrate observations at 75 m depth.
 Fig. F7 April distribution of nitrate observations at the surface.
 Fig. F8 April distribution of nitrate observations at 75 m depth.
 Fig. F9 May distribution of nitrate observations at the surface.
 Fig. F10 May distribution of nitrate observations at 75 m depth.
 Fig. F11 June distribution of nitrate observations at the surface.
 Fig. F12 June distribution of nitrate observations at 75 m depth.
 Fig. F13 July distribution of nitrate observations at the surface.
 Fig. F14 July distribution of nitrate observations at 75 m depth.
 Fig. F15 August distribution of nitrate observations at the surface.
 Fig. F16 August distribution of nitrate observations at 75 m depth.
 Fig. F17 September distribution of nitrate observations at the surface.
 Fig. F18 September distribution of nitrate observations at 75 m depth.
 Fig. F19 October distribution of nitrate observations at the surface.
 Fig. F20 October distribution of nitrate observations at 75 m depth.
 Fig. F21 November distribution of nitrate observations at the surface.
 Fig. F22 November distribution of nitrate observations at 75 m depth.
 Fig. F23 December distribution of nitrate observations at the surface.
 Fig. F24 December distribution of nitrate observations at 75 m depth.

Fig. F25 January mean nitrate (μM) at the surface.
 Fig. F26 January mean minus annual nitrate (μM) at the surface.
 Fig. F27 January mean nitrate (μM) at 75 m depth.
 Fig. F28 January mean minus annual nitrate (μM) at 75 m depth.
 Fig. F29 February mean nitrate (μM) at the surface.
 Fig. F30 February mean minus annual nitrate (μM) at the surface.
 Fig. F31 February mean nitrate (μM) at 75 m depth.
 Fig. F32 February mean minus annual nitrate (μM) at 75 m depth.
 Fig. F33 March mean nitrate (μM) at the surface.
 Fig. F34 March mean minus annual nitrate (μM) at the surface.
 Fig. F35 March mean nitrate (μM) at 75 m depth.
 Fig. F36 March mean minus annual nitrate (μM) at 75 m depth.
 Fig. F37 April mean nitrate (μM) at the surface.
 Fig. F38 April mean minus annual nitrate (μM) at the surface.
 Fig. F39 April mean nitrate (μM) at 75 m depth.
 Fig. F40 April mean minus annual nitrate (μM) at 75 m depth.
 Fig. F41 May mean nitrate (μM) at the surface.
 Fig. F42 May mean minus annual nitrate (μM) at the surface.
 Fig. F43 May mean nitrate (μM) at 75 m depth.
 Fig. F44 May mean minus annual nitrate (μM) at 75 m depth.
 Fig. F45 June mean nitrate (μM) at the surface.
 Fig. F46 June mean minus annual nitrate (μM) at the surface.
 Fig. F47 June mean nitrate (μM) at 75 m depth.
 Fig. F48 June mean minus annual nitrate (μM) at 75 m depth.
 Fig. F49 July mean nitrate (μM) at the surface.
 Fig. F50 July mean minus annual nitrate (μM) at the surface.
 Fig. F51 July mean nitrate (μM) at 75 m depth.
 Fig. F52 July mean minus annual nitrate (μM) at 75 m depth.
 Fig. F53 August mean nitrate (μM) at the surface.
 Fig. F54 August mean minus annual nitrate (μM) at the surface.
 Fig. F55 August mean nitrate (μM) at 75 m depth.
 Fig. F56 August mean minus annual nitrate (μM) at 75 m depth.
 Fig. F57 September mean nitrate (μM) at the surface.
 Fig. F58 September mean minus annual nitrate (μM) at the surface.
 Fig. F59 September mean nitrate (μM) at 75 m depth.
 Fig. F60 September mean minus annual nitrate (μM) at 75 m depth.
 Fig. F61 October mean nitrate (μM) at the surface.
 Fig. F62 October mean minus annual nitrate (μM) at the surface.

- Fig. F63 October mean nitrate (μM) at 75 m depth.
- Fig. F64 October mean minus annual nitrate (μM) at 75 m depth.
- Fig. F65 November mean nitrate (μM) at the surface.
- Fig. F66 November mean minus annual nitrate (μM) at the surface.
- Fig. F67 November mean nitrate (μM) at 75 m depth.
- Fig. F68 November mean minus annual nitrate (μM) at 75 m depth.
- Fig. F69 December mean nitrate (μM) at the surface.
- Fig. F70 December mean minus annual nitrate (μM) at the surface.
- Fig. F71 December mean nitrate (μM) at 75 m depth.
- Fig. F72 December mean minus annual nitrate (μM) at 75 m depth.

APPENDIX G

- Fig. G1. Annual distribution of silicate observations at the surface.
- Fig. G2. Annual distribution of silicate observations at 50 m depth.
- Fig. G3. Annual distribution of silicate observations at 75 m depth.
- Fig. G4. Annual distribution of silicate observations at 100 m depth.
- Fig. G5. Annual distribution of silicate observations at 150 m depth.
- Fig. G6. Annual distribution of silicate observations at 200 m depth.
- Fig. G7. Annual distribution of silicate observations at 250 m depth.
- Fig. G8. Annual distribution of silicate observations at 400 m depth.
- Fig. G9. Annual distribution of silicate observations at 500 m depth.
- Fig. G10. Annual distribution of silicate observations at 700 m depth.
- Fig. G11. Annual distribution of silicate observations at 1000 m depth.
- Fig. G12. Annual distribution of silicate observations at 1500 m depth.
- Fig. G13. Annual distribution of silicate observations at 2000 m depth.
- Fig. G14. Annual distribution of silicate observations at 2500 m depth.
- Fig. G15. Annual distribution of silicate observations at 3000 m depth.
- Fig. G16. Annual distribution of silicate observations at 4000 m depth.

- Fig. G17. Annual mean silicate (μM) at the surface.
- Fig. G18. Annual mean silicate (μM) at 50 m depth.
- Fig. G19. Annual mean silicate (μM) at 75 m depth.
- Fig. G20. Annual mean silicate (μM) at 100 m depth.
- Fig. G21. Annual mean silicate (μM) at 150 m depth.
- Fig. G22. Annual mean silicate (μM) at 200 m depth.
- Fig. G23. Annual mean silicate (μM) at 250 m depth.
- Fig. G24. Annual mean silicate (μM) at 400 m depth.
- Fig. G25. Annual mean silicate (μM) at 500 m depth.
- Fig. G26. Annual mean silicate (μM) at 700 m depth.
- Fig. G27. Annual mean silicate (μM) at 1000 m depth.
- Fig. G28. Annual mean silicate (μM) at 1500 m depth.
- Fig. G29. Annual mean silicate (μM) at 2000 m depth.
- Fig. G30. Annual mean silicate (μM) at 2500 m depth.
- Fig. G31. Annual mean silicate (μM) at 3000 m depth.
- Fig. G32. Annual mean silicate (μM) at 4000 m depth.

APPENDIX H

- Fig. H1. Winter (Jan.-Mar.) distribution of silicate observations at the surface.
- Fig. H2. Winter (Jan.-Mar.) distribution of silicate observations at 75 m depth.
- Fig. H3. Winter (Jan.-Mar.) distribution of silicate observations at 150 m depth.
- Fig. H4. Winter (Jan.-Mar.) distribution of silicate observations at 250 m depth.
- Fig. H5. Spring (Apr.-Jun.) distribution of silicate observations at the surface.
- Fig. H6. Spring (Apr.-Jun.) distribution of silicate observations at 75 m depth.
- Fig. H7. Spring (Apr.-Jun.) distribution of silicate observations at 150 m depth.
- Fig. H8. Spring (Apr.-Jun.) distribution of silicate observations at 250 m depth.
- Fig. H9. Summer (Jul.-Sep.) distribution of silicate observations at the surface.

Fig. H10. Summer (Jul.-Sep.) distribution of silicate observations at 75 m depth.
 Fig. H11. Summer (Jul.-Sep.) distribution of silicate observations at 150 m depth.
 Fig. H12. Summer (Jul.-Sep.) distribution of silicate observations at 250 m depth.
 Fig. H13. Fall (Oct.-Dec.) distribution of silicate observations at the surface.
 Fig. H14. Fall (Oct.-Dec.) distribution of silicate observations at 75 m depth.
 Fig. H15. Fall (Oct.-Dec.) distribution of silicate observations at 150 m depth.
 Fig. H16. Fall (Oct.-Dec.) distribution of silicate observations at 250 m depth.

Fig. H16. Winter (Jan.-Mar.) mean silicate (μM) at the surface.
 Fig. H17. Winter (Jan.-Mar.) minus annual mean silicate (μM) at the surface.
 Fig. H18. Winter (Jan.-Mar.) mean silicate (μM) at 75 m depth.
 Fig. H19. Winter (Jan.-Mar.) minus annual mean silicate (μM) at 75 m depth.
 Fig. H20. Winter (Jan.-Mar.) mean silicate (μM) at 150 m depth.
 Fig. H21. Winter (Jan.-Mar.) minus annual mean silicate (μM) at 150 m depth.
 Fig. H22. Winter (Jan.-Mar.) mean silicate (μM) at 250 m depth.
 Fig. H23. Winter (Jan.-Mar.) minus annual mean silicate (μM) at 250 m depth.
 Fig. H24. Spring (Apr.-Jun.) mean silicate (μM) at the surface.
 Fig. H25. Spring (Apr.-Jun.) minus annual mean silicate (μM) at the surface.
 Fig. H26. Spring (Apr.-Jun.) mean silicate (μM) at 75 m depth.
 Fig. H27. Spring (Apr.-Jun.) minus annual mean silicate (μM) at 75 m depth.
 Fig. H28. Spring (Apr.-Jun.) mean silicate (μM) at 150 m depth.
 Fig. H29. Spring (Apr.-Jun.) minus annual mean silicate (μM) at 150 m depth.
 Fig. H30. Spring (Apr.-Jun.) mean silicate (μM) at 250 m depth.
 Fig. H31. Spring (Apr.-Jun.) minus annual mean silicate (μM) at 250 m depth.
 Fig. H32. Summer (Jul.-Sep.) mean silicate (μM) at the surface.
 Fig. H33. Summer (Jul.-Sep.) mean minus annual silicate (μM) at the surface.
 Fig. H34. Summer (Jul.-Sep.) mean silicate (μM) at 75 m depth.
 Fig. H35. Summer (Jul.-Sep.) mean minus annual silicate (μM) at 75 m depth.
 Fig. H36. Summer (Jul.-Sep.) mean silicate (μM) at 150 m depth.
 Fig. H37. Summer (Jul.-Sep.) mean minus annual silicate (μM) at 150 m depth.
 Fig. H38. Summer (Jul.-Sep.) mean silicate (μM) at 250 m depth.
 Fig. H39. Summer (Jul.-Sep.) mean minus annual silicate (μM) at 250 m depth.
 Fig. H40. Fall (Oct.-Dec.) mean silicate (μM) at the surface.
 Fig. H41. Fall (Oct.-Dec.) mean minus annual silicate (μM) at the surface.
 Fig. H42. Fall (Oct.-Dec.) mean silicate (μM) at 75 m depth.
 Fig. H43. Fall (Oct.-Dec.) mean minus annual silicate (μM) at 75 m depth.
 Fig. H44. Fall (Oct.-Dec.) mean silicate (μM) at 150 m depth.
 Fig. H45. Fall (Oct.-Dec.) mean minus annual silicate (μM) at 150 m depth.
 Fig. H46. Fall (Oct.-Dec.) mean silicate (μM) at 250 m depth.
 Fig. H47. Fall (Oct.-Dec.) mean minus annual silicate (μM) at 250 m depth.

APPENDIX I

Fig. I1. January distribution of silicate observations at the surface.
 Fig. I2. January distribution of silicate observations at 75 m depth.
 Fig. I3. February distribution of silicate observations at the surface.
 Fig. I4. February distribution of silicate observations at 75 m depth.
 Fig. I5. March distribution of silicate observations at the surface.
 Fig. I6. March distribution of silicate observations at 75 m depth.
 Fig. I7. April distribution of silicate observations at the surface.
 Fig. I8. April distribution of silicate observations at 75 m depth.
 Fig. I9. May distribution of silicate observations at the surface.
 Fig. I10. May distribution of silicate observations at 75 m depth.
 Fig. I11. June distribution of silicate observations at the surface.
 Fig. I12. June distribution of silicate observations at 75 m depth.
 Fig. I13. July distribution of silicate observations at the surface.
 Fig. I14. July distribution of silicate observations at 75 m depth.
 Fig. I15. August distribution of silicate observations at the surface.

Fig. I16 August distribution of silicate observations at 75 m depth.
 Fig. I17 September distribution of silicate observations at the surface.
 Fig. I18 September distribution of silicate observations at 75 m depth.
 Fig. I19 October distribution of silicate observations at the surface.
 Fig. I20 October distribution of silicate observations at 75 m depth.
 Fig. I21 November distribution of silicate observations at the surface.
 Fig. I22 November distribution of silicate observations at 75 m depth.
 Fig. I23 December distribution of silicate observations at the surface.
 Fig. I24 December distribution of silicate observations at 75 m depth.

Fig. I25 January mean silicate (μM) at the surface.
 Fig. I26 January mean minus annual silicate (μM) at the surface.
 Fig. I27 January mean silicate (μM) at 75 m depth.
 Fig. I28 January mean minus annual silicate (μM) at 75 m depth.
 Fig. I29 February mean silicate (μM) at the surface.
 Fig. I30 February mean minus annual silicate (μM) at the surface.
 Fig. I31 February mean silicate (μM) at 75 m depth.
 Fig. I32 February mean minus annual silicate (μM) at 75 m depth.
 Fig. I33 March mean silicate (μM) at the surface.
 Fig. I34 March mean minus annual silicate (μM) at the surface.
 Fig. I35 March mean silicate (μM) at 75 m depth.
 Fig. I36 March mean minus annual silicate (μM) at 75 m depth.
 Fig. I37 April mean silicate (μM) at the surface.
 Fig. I38 April mean minus annual silicate (μM) at the surface.
 Fig. I39 April mean silicate (μM) at 75 m depth.
 Fig. I40 April mean minus annual silicate (μM) at 75 m depth.
 Fig. I41 May mean silicate (μM) at the surface.
 Fig. I42 May mean minus annual silicate (μM) at the surface.
 Fig. I43 May mean silicate (μM) at 75 m depth.
 Fig. I44 May mean minus annual silicate (μM) at 75 m depth.
 Fig. I45 June mean silicate (μM) at the surface.
 Fig. I46 June mean minus annual silicate (μM) at the surface.
 Fig. I47 June mean silicate (μM) at 75 m depth.
 Fig. I48 June mean minus annual silicate (μM) at 75 m depth.
 Fig. I49 July mean silicate (μM) at the surface.
 Fig. I50 July mean minus annual silicate (μM) at the surface.
 Fig. I51 July mean silicate (μM) at 75 m depth.
 Fig. I52 July mean minus annual silicate (μM) at 75 m depth.
 Fig. I53 August mean silicate (μM) at the surface.
 Fig. I54 August mean minus annual silicate (μM) at the surface.
 Fig. I55 August mean silicate (μM) at 75 m depth.
 Fig. I56 August mean minus annual silicate (μM) at 75 m depth.
 Fig. I57 September mean silicate (μM) at the surface.
 Fig. I58 September mean minus annual silicate (μM) at the surface.
 Fig. I59 September mean silicate (μM) at 75 m depth.
 Fig. I60 September mean minus annual silicate (μM) at 75 m depth.
 Fig. I61 October mean silicate (μM) at the surface.
 Fig. I62 October mean minus annual silicate (μM) at the surface.
 Fig. I63 October mean silicate (μM) at 75 m depth.
 Fig. I64 October mean minus annual silicate (μM) at 75 m depth.
 Fig. I65 November mean silicate (μM) at the surface.
 Fig. I66 November mean minus annual silicate (μM) at the surface.
 Fig. I67 November mean silicate (μM) at 75 m depth.
 Fig. I68 November mean minus annual silicate (μM) at 75 m depth.
 Fig. I69 December mean silicate (μM) at the surface.
 Fig. I70 December mean minus annual silicate (μM) at the surface.
 Fig. I71 December mean silicate (μM) at 75 m depth.
 Fig. I72 December mean minus annual silicate (μM) at 75 m depth.

Preface

The oceanographic analyses described by this atlas series expand on earlier works, *e.g.* the *World Ocean Atlas 1998* (WOA98), *World Ocean Atlas 1994* (WOA94) and *Climatological Atlas of the World Ocean*. Previously published oceanographic objective analyses have proven to be of great utility to the oceanographic, climate research, and operational environmental forecasting communities. Such analyses are used as boundary and/or initial conditions in numerical ocean circulation models and atmosphere-ocean models, for verification of numerical simulations of the ocean, as a form of "sea truth" for satellite measurements such as altimetric observations of sea surface height, for computation of nutrient fluxes by Ekman transport, and for planning oceanographic expeditions.

We have expanded our earlier analyses to include an all-data annual analysis of chlorophyll, monthly analyses of oxygen, and seasonal and monthly analyses of nutrients. Additional data for these variables have become available and there is a need for such analyses of these data in order to:

- 1) study the role of biogeochemical cycles in determining how the earth's climate system works, particularly the vulnerability of ocean ecosystems to climate change (IPCC, 1996);
- 2) help verify remotely sensed estimates of chlorophyll (SeaWiFS, ADEOS missions) which requires knowledge of *in situ* variables such as chlorophyll and plankton;
- 3) provide the most comprehensive set of oceanographic databases and products based on these data to the international research and forecasting communities.

We continue preparing climatological analyses on a one-degree grid. This is because higher resolution analyses are not justified for all the variables we are working with and we wish to produce a set of analyses for which all variables have been analyzed in the same manner. High-resolution analyses as typified by the work of Boyer and Levitus (1997) will be published as separate atlases.

In the acknowledgment section of this publication we have expressed our view that creation of global ocean profile and plankton databases and analyses are only possible through the cooperation of scientists, data managers, and scientific administrators throughout the international scientific community. I would also like to thank my colleagues and the staff of the Ocean Climate Laboratory of NODC for their dedication to the project leading to publication of this atlas series. Their integrity and thoroughness have made this database possible. It is my belief that the development and management of national and international oceanographic data archives is best performed by scientists who are actively working with the historical data.

Sydney Levitus
National Oceanographic Data Center
Silver Spring, MD
May 2002

Acknowledgments

This work was made possible by a grant from the NOAA Climate and Global Change Program which enabled the establishment of a research group at the National Oceanographic Data Center. The purpose of this group is to prepare research quality oceanographic databases, as well as to compute objective analyses of, and diagnostic studies based on, these databases.

The data on which this atlas is based are in *World Ocean Database 2001* and are distributed on-line and CD-ROM by NODC/WDC. Many data were acquired as a result of the NODC *Oceanographic Data Archaeology and Rescue* (NODAR) project, the IOC/IODE *Global Oceanographic Data Archaeology and Rescue* (GODAR) project, and the IOC/IODE *World Ocean Database* project (WOD). At NODC/WDC, “data archaeology and rescue” projects are supported with funding from the NOAA Environmental Science Data and Information Management (ESDIM) Program and the NOAA Climate and Global Change Program which has included support from NASA and DOE. Support for some of the regional IOC/GODAR meetings was provided by the MAST program of the European Union. The European Community has also provided support for the MEDAR/MEDATLAS project which has resulted in the inclusion of substantial amounts of ocean profile data from the Mediterranean and Black Seas into *World Ocean Database 2001*.

We would like to acknowledge the scientists, technicians, and programmers who have submitted data to national and regional data centers as well as the managers and staff at the various data centers. Their efforts have made this and similar works possible.

WORLD OCEAN ATLAS 2001

VOLUME 4: Nutrients

*Margarita E. Conkright, Hernan E. Garcia, Todd D. O'Brien, Ricardo A. Locarnini,
Timothy P. Boyer, Cathy Stephens, and John I. Antonov*
National Oceanographic Data Center
Silver Spring, MD

ABSTRACT

This atlas contains global maps of the climatological distributions of phosphate, nitrate, and silicate at selected standard depth levels on a one-degree grid. Maps for all-data annual, seasonal, and monthly compositing periods are presented at standard depth levels. Seasonal and monthly difference (from the annual mean) fields are also presented for phosphate, nitrate, and silicate at selected standard depth levels. The fields used to generate these maps were computed by objective analysis of historical data. Data distribution maps are presented for all-data annual, seasonal and monthly compositing periods at selected standard levels. Nutrient data are particularly sparse for the climatological monthly compositing periods. However, due to intense interest in these fields, we present both analyses and data distribution plots by months. As with all maps showing the results of our objective analyses, hatching indicates regions in which data are too sparse to produce a representative analysis and our analysis mainly represent the first-guess field used. These fields show the current state of the distribution of nutrient data, and the need for additional data. As more data are received, we will improve on the quality and representativeness of the annual, seasonal, and monthly climatological fields.

1. INTRODUCTION

This atlas is an analysis of all historical nutrient profile data available from the National Oceanographic Data Center (NODC) and World Data Center (WDC) for Oceanography, Silver Spring, Maryland. Many data have been acquired as a result of several data management projects including:

- a) the Intergovernmental Oceanographic Commission (IOC) *Global Oceanographic Data Archaeology and Rescue* (GODAR) project;
- b) the NODC *Oceanographic Data Archaeology and Rescue* (NODAR) project;
- c) the IOC *World Ocean Database* project (WOD);
- d) the IOC *Global Temperature Salinity Profile Project*.

Data used in this atlas have been analyzed in a consistent, objective manner on a one-degree latitude-longitude grid at standard oceanographic levels between the surface and ocean bottom to a maximum depth of 5500m. The procedures are identical to those used in *World Ocean Atlas 1998* (WOA98) (Conkright *et al.*, 1998) and similar to those used to produce earlier analyses (Levitus, 1982; Conkright *et al.*, 1994a). Annual, seasonal and monthly analyses have been computed for phosphate, nitrate, and silicate.

Objective analyses shown in this atlas are limited by the nature of the data base (data are non-synoptic and scattered in space), characteristics of the objective analysis

techniques, and the grid used. These limitations and characteristics will be discussed below.

Since the publication of WOA98, substantial amounts of additional historical data have become available. However, even with these additional data, we are still hampered in a number of ways by a lack of data. Because of the lack of data, we are forced to examine the annual cycle by compositing all data regardless of the year of observation. In some areas, quality control is made difficult by the limited number of data. Data may exist in an area for only one season, thus precluding any representative annual analysis. In some areas there may be a reasonable spatial distribution of data points on which to base an analysis, but there may be only a few (perhaps only one) data in each one-degree latitude-longitude square.

2. DATA AND DATA DISTRIBUTION

Data sources and quality control procedures are briefly described below. For further information on the data sources used in *World Ocean Atlas 2001* (WOA01) refer to the World Ocean Database 2001 (WOD01) series (Conkright *et al.*, 2002a). The quality control procedures we have used in preparing these analyses are described by Conkright *et al.* (2002b).

2.1 Data sources

Historical Ocean Station Data (OSD) nutrient profiles used in this atlas are from the NODC/WDC archives and

includes all data gathered as a result of the NODAR, GODAR, and WOD projects.

Appendix A shows the geographic distribution of all historical phosphate observations at selected standard depth levels, Appendix B shows the distribution for individual seasons and Appendix C for individual months. Appendix D shows the geographic distribution of all historical nitrate observations at selected standard depth levels, Appendix E shows the distribution for individual seasons, and Appendix F for individual months. Appendix G shows the geographic distribution of all historical silicate observations at selected standard depth levels, Appendix H shows the distribution for individual seasons, and Appendix I for individual months. In all data distribution maps that appear in the appendices, a small dot indicates a one-degree square containing one to four observations and a large dot indicates a square containing five or more observations.

We define the terms "standard level data" and "observed level data" here so the reader can understand the various data distribution figures, summary figures, and tables we present in this atlas. We refer to the actual measured value of an oceanographic variable *in situ* (Latin for "in place") as an "observation," and to the depth at which such a measurement was made as the "observed level depth." We may refer to such data as "observed level data." Before the development of oceanographic instrumentation that measure at high frequencies in the vertical, oceanographers often attempted to make measurements at selected "standard levels" in the water column. Sverdrup *et al.* (1942) presented the suggestions of the International Association of Physical Oceanography (IAPSO) as to which depths oceanographic measurements should be made or interpolated to for analysis. Different nations or institutions have a slightly different set of standard levels defined. For many purposes, including preparation of this atlas, observed level data are interpolated to standard observation levels, if such data do not occur exactly at a standard observation levels. We have prepared objective analyses at the NODC standard levels as given in Table 1 and added levels at 3500, 4500, and 5500. Section 3.1 discusses the vertical interpolation procedures used in our work.

2.2 Data quality control

Quality control of the data is a major task, the difficulty of which is directly related to lack of data (in some areas) upon which to base statistical checks. Consequently certain empirical criteria were applied, and as part of the last processing step, subjective judgment was used. Individual data, and in some cases entire profiles or cruises, have been flagged because these data produced features that were judged to be non-representative or in error. As part of our work, we have made available WOD01 which contains both observed level profile data as well as standard level profile data with various quality control flags applied. Our knowledge of the variability of the world ocean now includes a greater appreciation and understanding of the

ubiquity of eddies, rings, and lenses in some parts of the world ocean as well as interannual and interdecadal variability of water mass properties associated with modal variability of the atmosphere such as the North Atlantic Oscillation and El Niño Southern Ocean Oscillation. Therefore, we have simply flagged data, not eliminated them. Thus, individual investigators can make their own decision regarding the representativeness or correctness of the data. Investigators studying the distribution of features such as eddies will be interested in those data that we may regard as unrepresentative for the preparation of the analyses shown in this atlas.

2.2a Duplicate elimination

Because data are received from many sources, sometimes the same data set is received at NODC/WDC more than once but with slightly different time and/or position and/or data values, and hence are not easily identified as duplicate stations. Therefore, our databases were checked for the presence of exact and "near" exact replicates using eight different criteria. The first checks involve identifying stations with exact position/date/time and data values; the next checks involve offsets in position/date/time. Profiles identified as duplicates in the checks with a large offset were individually verified to ensure they were indeed duplicate profiles.

All but one profile from each set of replicate profiles were eliminated at the first step of our processing.

2.2b Range checks and gradient checks

Range checking (checking whether data is within set minimum and maximum values as a function of depth) was performed on all data as a first error check to flag and eliminate from further use the relatively few data that seemed to be grossly in error. Range checks were prepared for individual regions of the world ocean. Conkright *et al.* (2002b) and Conkright *et al.* (1994b) detail the quality control procedures and include tables showing the ranges selected for each basin.

A check as to whether excessive gradients occur in the data were made for each variable in WOD01 both in terms of positive and negative gradients.

2.2c Statistical checks

Statistical checks were performed as follows. All data for each variable (irrespective of season), at each standard level, were averaged by five-degree latitude-longitude squares to produce a record of the number of observations, mean, and standard deviation in each square. Statistics were computed for the annual, seasonal, and monthly compositing periods. Below 50 m depth, if data were more than three standard deviations from the mean, the data were flagged and eliminated from further use in our objective analyses. Above 50 m depth, a five-standard-deviation

criterion was used in five-degree squares that contained any land area. In selected five degree squares that are close to land areas, a four standard-deviation check was used. In all other squares a three standard-deviation criterion was used.

The reason for the weaker criterion in coastal and near-coastal regions is the exceptionally large variability in the coastal five-degree square statistics for some variables. Frequency distributions of some variables in some coastal regions are observed to be skewed or bimodal. Thus to avoid eliminating possibly good data in highly variable environments, the standard deviation criteria were weakened.

The total number of nutrient measurements in each cast, as well as the total number of observations exceeding the criterion, were recorded. If more than two observations in a cast were found to exceed the standard deviation criterion, then the entire cast was flagged. This check was imposed after tests indicated that surface data from particular casts (which upon inspection appeared to be erroneous) were being flagged but deeper data were not. Other situations were found where erroneous data from the deeper portion of a cast were flagged, while near-surface data from the same cast were not flagged because of larger natural variability in surface layers. One reason for this was the decrease of the number of observations with depth and the resulting change in sample statistics. The standard-deviation check was applied twice to the data set for each compositing period. Individual flags were set for each period.

In summary, first the five-degree square statistics were computed, and the elimination procedure described above was used to provide a preliminary data set. Next, new five-degree-square statistics were computed from this preliminary data set and used with the same statistical check to produce a new, "clean" data set. The reason for applying the statistical check twice was to flag (and eliminate from further use), in the first round, any grossly erroneous or non-representative data from the data set that would artificially increase the variances. The second check is then more effective in eliminating smaller, but still erroneous or non-representative, observations. The standard deviation for phosphate observations at 500 meters depth on a one-degree latitude-longitude square is shown in Figure 1a; the standard error of the mean for the same depth is shown in Figure 1b.

2.2d Subjective flagging of data

The data were averaged by one-degree squares for input to the objective analysis program. After initial objective analyses were computed, the input set of one-degree means still contained suspicious data contributing to unrealistic distributions, yielding intense bull's-eyes or gradients. Examination of these features indicated that some of them were due to particular oceanographic cruises. In such cases, data from an entire cruise were eliminated from further use by setting a flag on each profile from the cruise. In other

cases, individual profiles or measurements were found to cause these features and were eliminated from use.

2.2e Representativeness of the data

Another quality control issue is data representativeness. The general paucity of data forces the compositing of all historical data to produce "climatological" fields. In a given one-degree square, there may be data from a month or season of one particular year, while in the same or a nearby square there may be data from an entirely different year. If there is large interannual variability in a region where scattered sampling in time has occurred, then one can expect the analysis to reflect this. Because the observations are scattered randomly with respect to time, except for a few limited areas, the results cannot, in a strict sense, be considered a true long-term climatological average.

We present smoothed analyses of historical means, based (in certain areas) on relatively few observations. We believe, however, that useful information about the oceans can be gained through our procedures and that the large-scale features are representative of the real ocean. We believe that, if a hypothetical global synoptic set of ocean data (nutrients) existed, and one were to smooth this data to the same degree as we have smoothed the historical means overall, the large-scale features would be similar to our results. Some differences would certainly occur because of interannual-to-decadal-scale variability.

To clarify discussions of the amount of available data, quality control techniques, and representativeness of the data, the reader should examine in detail the maps showing the distribution of data (Appendices A-I) and the *World Ocean Database 2001* atlas series which shows the distribution of oceanographic stations as a function of year and instrument type. These maps are provided to give the reader a quick, simple way of examining the historical data distributions. Basically, the data diminish in number with increasing depth. In the upper ocean, the all-data annual mean distributions are quite good for defining large-scale features, but for the seasonal periods, the data base is inadequate for some regions. With respect to the deep ocean, in some areas the distribution of observations may be adequate for some diagnostic computations but inadequate for other purposes. If an isolated deep basin or some region of the deep ocean has only one observation, then no horizontal gradient computations are meaningful. However, useful information is provided by the observation in the computation of other quantities (e.g., a volumetric mean over a major ocean basin).

3. DATA PROCESSING PROCEDURES

3.1 Vertical interpolation to standard levels

Vertical interpolation of observed level data to standard levels followed procedures in JPOTS Editorial Panel

(1991). These procedures are in part based on the work of Reiniger and Ross (1968). Four observed level values surrounding the standard level values were used, two values from above the standard level and two values below the standard level. The pair of values furthest from the standard level are termed “exterior” points and the pair of values closest to the standard level are termed “interior” points. Paired parabolas were generated via Lagrangian interpolation. A reference curve was fitted to the four data points and used to define unacceptable interpolations caused by "overshooting" in the interpolation. When there were too few data points above or below the standard level to apply the Reiniger and Ross technique, we used a three-point Lagrangian interpolation. If three points were not available (either two above and one below or vice-versa), we used linear interpolation. In the event that an observation occurred exactly at the depth of a standard level, then a direct substitution was made. Table 1 provides the range of acceptable distances for which observed level data could be used for interpolation to a standard level.

3.2 Methods of analysis

3.2a Overview

An objective analysis scheme of the type described by Barnes (1964) was used to produce the fields shown in this atlas. This scheme had its origins in the work of Cressman (1959). In *World Ocean Atlas 1994* (WOA94), the Barnes (1973) scheme was used. This required only one "correction" to the first-guess field at each grid point in comparison to the successive correction method of Cressman (1959) and Barnes (1964). This was to minimize computer time used in the processing. Barnes (1994) recommends a return to a multi-pass analysis when computer time is not an issue. Based on our own experience we agree with this assessment. The single pass analysis, used in WOA94, caused an artificial front in the Southeastern Pacific Ocean in a data sparse area (Anne Marie Treguier, personal communication). The analysis scheme used in generating WOA98 and WOA01 analyses uses a three-pass “correction” which eliminates this artificial front.

Inputs to the analysis scheme were one-degree square means of data values at standard levels (for whatever period and variable being analyzed), and a first-guess value for each square. For instance, one-degree square means for our annual analysis were computed using all available data regardless of date of observation. For July, we used all historical July data regardless of year of observation.

Analysis was the same for all standard depth levels. Each one-degree latitude-longitude square value was defined as being representative of its square. The 360x180 gridpoints are located at the intersection of half-degree lines of latitude and longitude. An influence radius was then specified. At those grid points where there was an observed mean value, the difference between the mean and the first-guess field

was computed. Next, a correction to the first-guess value at all gridpoints was computed as a distance-weighted mean of all gridpoint difference values that lie within the area around the gridpoint defined by the influence radius. Mathematically, the correction factor derived by Barnes (1964) is given by the expression

$$C_{i,j} = \frac{\sum_{s=1}^n W_s Q_s}{\sum_{s=1}^n W_s} \quad (1)$$

in which

(i,j) = coordinates of a gridpoint in the east-west and north-south directions respectively;

$C_{i,j}$ = the correction factor at gridpoint coordinates (i,j);

n = the number of observations that fall within the area around the point i,j defined by the influence radius;

Q_s = the difference between the observed mean and the first-guess at the S^{th} point in the influence area;

**$W_s = \exp(-E r^2 R^{-2})$ for $r \leq R$;
0 for $r > R$;**

r = distance of the observation from the gridpoint;

R = influence radius;

E = 4.

The derivation of the weight function, W_s , will be presented in the following section. At each gridpoint we computed an analyzed value $G_{i,j}$ as the sum of the first-guess, $F_{i,j}$, and the correction $C_{i,j}$. The expression for this is

$$G_{i,j} = F_{i,j} + C_{i,j} \quad (2)$$

If there were no data points within the area defined by the influence radius, then the correction was zero, the first-guess field was left unchanged, and the analyzed value was simply the first-guess value. This correction procedure was applied at all gridpoints to produce an analyzed field. The resulting field was first smoothed with a median filter (Tukey, 1974; Rabiner *et al.*, 1975) and then smoothed with a five-point smoother of the type described by Shuman (1957). The choice of first-guess fields is important and we discuss our procedures in section 3.2e.

The analysis scheme is based on the work of several researchers analyzing meteorological data. Bergthorsson and Doos (1955) computed corrections to a first-guess field using various techniques: one assumed that the difference between a first-guess value and an analyzed value at a gridpoint was the same as the difference between an observation and a first-guess value at a nearby observing station. All the observed differences in an area surrounding the gridpoint were then averaged and added to the gridpoint first-guess value to produce an analyzed value. Cressman (1959) applied a distance-related weight function to each observation used in the correction in order to give more weight to observations that occur closest to the gridpoint. In addition, Cressman introduced the method of performing several iterations of the analysis scheme using the analysis produced in each iteration as the first-guess field for the next iteration. He also suggested starting the analysis with a relatively large influence radius and decreasing it with successive iterations so as to analyze smaller scale phenomena with each pass.

Sasaki (1960) introduced a weight function that was specifically related to the density of observations, and Barnes (1964, 1973) extended the work of Sasaki. The weight function of Barnes (1964) has been used here. The objective analysis scheme we used is in common use by the mesoscale meteorological community. Several studies of objective analysis techniques have been made. Achtemeier (1987) examined the "concept of varying influence radii for a successive corrections objective analysis scheme." Seaman (1983) compared the "objective analysis accuracies of statistical interpolation and successive correction schemes." Smith and Leslie (1984) performed an "error determination of a successive correction type objective analysis scheme." Smith *et al.* (1986) made "a comparison of errors in objectively analyzed fields for uniform and non-uniform station distribution."

3.2b Derivation of Barnes (1964) weight function

The principle upon which Barnes' (1964) weight function is derived is that "the two-dimensional distribution of an atmospheric variable can be represented by the summation of an infinite number of independent harmonic waves, that is, by a Fourier integral representation". If $f(x,y)$ is the variable, then in polar coordinates (r,θ) , a smoothed or filtered function $h(x,y)$ can be defined:

$$h(x,y) = \frac{1}{2\pi} \int_0^{2\pi} \int_0^{\infty} \eta f(x + r\cos\theta, y + r\sin\theta) d(r^2 / 4K) d\theta \quad (3)$$

in which r is the radial distance from a gridpoint whose coordinates are (x,y) . The weight function is defined as

$$\eta = \exp(-r^2 / 4K) \quad (4)$$

which resembles the Gaussian distribution. The shape of the weight function is determined by the value of K , which depends on the distribution of data. The determination of K follows. The weight function has the property that

$$\frac{1}{2\pi} \int_0^{2\pi} \int_0^{\infty} \eta d\left(\frac{r^2}{4K}\right) d\theta = 1. \quad (5)$$

This property is desirable because in the continuous case (3) the application of the weight function to the distribution $f(x,y)$ will not change the mean of the distribution. However, in the discrete case (1), we only sum the contributions to within the distance R . This introduces an error in the evaluation of the filtered function, because the condition given by (5) does not apply. The error can be pre-determined and set to a reasonably small value in the following manner. If one carries out the integration in (5) with respect to θ , the remaining integral can be rewritten as

$$\int_0^R \eta d\left(\frac{r^2}{4K}\right) + \int_R^{\infty} \eta d\left(\frac{r^2}{4K}\right) = 1. \quad (6)$$

Defining the second integral as ε yields

$$\int_0^R \exp\left(-\frac{r^2}{4K}\right) d\left(\frac{r^2}{4K}\right) = 1 - \varepsilon \quad (7)$$

from which

$$\varepsilon = \exp(-R^2 / 4K)$$

Levitus (1982) chose $\varepsilon = 0.02$, which implies with respect to (6) the representation of 98 percent of the influence of any data around the gridpoint in the area defined by the influence radius, R . In terms of the weight function used in the evaluation of (1) this choice leads to a value of $E=4$ since

$$E = R^2 / 4K = -\ln \varepsilon.$$

Thus,

$$K = R^2 / 16.$$

The choice of ε and the specification of R determine the shape of the weight function.

Barnes (1964) proposed using this scheme in an iterative fashion similar to Cressman (1959). Levitus (1982) used a four iteration scheme with a variable influence radius for each pass. Conkright *et al.* (1994a) used a one-iteration scheme. WOA98 and WOA01 use a three iteration scheme with a variable influence radius. The three influence radii are 888, 666, and 444 km.

3.2c Derivation of Barnes (1964) response function

It is desirable to know the response of a data set to the interpolation procedure applied to it. Following Barnes (1964) we let

$$f(x) = A \sin(ax) \quad (8)$$

in which $a = 2\pi/\lambda$ with λ being the wavelength of a particular Fourier component, and substitute this function into equation (3) along with the expression for η in equation (4). Then

$$g(x) = D(A \sin(ax)) = Df(x) \quad (9)$$

in which D is the response function for one application of the analysis. The phase of each Fourier component is not changed by the interpolation procedure. The results of an analysis pass are used as the first-guess for the next analysis pass in an iterative fashion. The response function after N iterations as derived by Barnes (1964) is

$$g_n = f(x) D \sum_{n=1}^{N-1} (1 - D)^{n-1} \quad (10)$$

Equation (10) differs trivially from that given by Barnes. The difference is due to our first-guess field being defined as a zonal average, annual mean, seasonal mean, or monthly mean, whereas Barnes used the first application of the analysis as a first-guess. Barnes (1964) also showed that applying the analysis scheme in an iterative fashion will result in convergence of the analyzed field to the observed data field. However, it is not desirable to approach the observed data too closely, because at least seven or eight gridpoints are needed to represent a Fourier component.

The response function given in (10) is useful in two ways: it is informative to know what Fourier components make up the analyses, and the computer programs used in generating the analyses can be checked for correctness by comparison with (10).

3.2d Choice of response function

The distribution of observations (see appendices) at different depths and for the different averaging periods, are not regular in space or time. At one extreme, regions exist in which every one-degree square contains data and no interpolation needs to be performed. At the other extreme are regions in which few if any data exist. Thus, with variable data spacing the average separation distance between gridpoints containing data is a function of geographical position and averaging period. However, if we computed and used a different average separation distance for each variable at each depth and each averaging period,

we would be generating analyses in which the wavelengths of observed phenomena might differ from one depth level to another and from one season to another. In WOA94, a fixed influence radius of 555 kilometers was used to allow uniformity in the analysis of all variables. For these analyses, a three-pass analysis, based on Barnes (1964), with influence radii of 888, 666 and 444 km was used.

Inspection of (1) shows that the difference between the analyzed field and the first-guess at any gridpoint is proportional to the sum of the weighted-differences between the observed mean and first-guess at all gridpoints containing data within the influence area.

The reason for using the five-point smoother and the median smoother is that our data are not evenly distributed in space. As the analysis moves from regions containing data to regions devoid of data, small-scale discontinuities may develop. The five-point and median smoothers are used to eliminate these discontinuities. The five-point smoother does not affect the phase of the Fourier components that comprise an analyzed field.

The response function for the analyses presented in this atlas and in WOA98 is given in Table 2 and Figure 2. For comparison purposes, the response function used by Levitus (1982) and Conkright *et al.* (1994a) are also presented. The response function represents the smoothing inherent in the objective analysis described above plus the effects of one application of the five-point smoother and one application of a five-point median smoother. The effect of varying the amount of smoothing in North Atlantic sea surface temperature (SST) fields has been quantified by Levitus (1982) for a particular case. In a region of strong SST gradient such as the Gulf Stream, the effect of smoothing can easily be responsible for differences between analyses exceeding 1.0 °C.

To avoid the problem of the influence region extending across land or sills to adjacent basins, the objective analysis program uses basin "identifiers" to preclude the use of data from adjacent basins. Table 3 lists these basins and the depth at which no exchange of information between basins is allowed during the objective analysis of data, i.e., "depths of mutual exclusion." Some regions are nearly, but not completely, isolated topographically. Because some of these nearly isolated basins have water mass properties that are different from surrounding basins, we have chosen to treat these as isolated basins as well. Not all such basins have been identified because of the complicated structure of the sea floor. In Table 3, a region marked with an "*" can interact with adjacent basins except for special areas such as the Isthmus of Panama.

3.2e First-guess field determination

There are gaps in the data coverage, and in some parts of the world ocean, there exist adjacent basins whose water mass properties are individually nearly homogeneous but

have distinct basin-to-basin differences. Spurious features can be created when an influence area extends over two basins of this nature (basins are listed in Table 3). Our choice of first-guess field attempts to minimize the creation of these features. To provide a first-guess field for the annual analysis at any standard level, we first zonally averaged the observed data in each one-degree latitude belt by individual ocean basins.

An annual analysis of a variable was then used as the first-guess for each seasonal analysis and each seasonal analysis was used as a first-guess for the appropriate monthly analysis if computed.

We then reanalyzed the data for each variable using the newly produced analyses as first-guess fields described as follows and as shown in Figure 3. A new annual mean was computed as the mean of the twelve monthly analyses for the upper 500m, and the mean of the four seasons below 500 m depth. This new annual mean was used as the first-guess field for new seasonal analyses. These new seasonal analyses were used to produce new monthly analyses. This procedure produces slightly smoother means. More importantly we recognize that fairly large data-void regions exist, in some cases to such an extent that a seasonal or monthly analysis in these regions is not meaningful. We are interested in computing integral quantities such as heat storage that are deviations from annual means. Geographic distribution of observations for the all-data annual periods (see appendices) is excellent for upper layers of the ocean. By using an all-data annual mean, first-guess field regions where data exists for only one season or month will show no contribution to the annual cycle. By contrast, if we used a zonal average for each season or month, then, in those latitudes where gaps exist, the first-guess field would be heavily biased by the few data points that exist. If these were anomalous data in some way, an entire basin-wide belt might be affected.

One advantage of producing "global" fields for a particular compositing period (even though some regions are data void) is that such analyses can be modified by investigators for use in modeling studies. For example, England (1992) noted that the temperature distribution produced by Levitus (1982) for the Antarctic is too high (due to a lack of winter data for the Southern Hemisphere) to allow for the formation of Antarctic Intermediate Water in an ocean general circulation model. By increasing the temperature of the "observed" field the model was able to produce this water mass.

3.3 Choice of objective analysis procedures

Optimum interpolation (Gandin, 1963) has been used by some investigators to objectively analyze oceanographic data. We recognize the power of this technique but have not used it to produce analyzed fields. As described by Gandin (1963), optimum interpolation is used to analyze synoptic data using statistics based on historical data. In particular,

second-order statistics such as correlation functions are used to estimate the distribution of first order parameters such as means. We attempt to map most fields in this atlas based on relatively sparse data sets. By necessity we must composite all data regardless of year of observation, to have enough data to produce a global, hemispheric, or regional analysis for a particular month, season, or even yearly. Because of the paucity of data, we prefer not to use an analysis scheme that is based on second order statistics. In addition, as Gandin has noted, there are two limiting cases associated with optimum interpolation. The first is when a data distribution is dense. In this case, the choice of interpolation scheme makes little difference. The second case is when data are sparse. In this case, an analysis scheme based on second order statistics is of questionable value. For additional information on objective analysis procedures see Thiebaut and Pedder (1987) and Daley (1991).

3.4 Choice of spatial grid

The analyses that comprise WOA01 and WOA98 have been computed using a new land-sea topography to define ocean depths at each grid point (ETOPO5, 1988). From the ETOPO5 land mask, a quarter-degree land mask was created based on ocean bottom depth and land criteria. If four or more 5-minute square values out of a possible nine in a one-quarter-degree box were defined as land, then the quarter-degree gridbox was defined to be land. If no more than two of the 5-minute squares had the same depth value in a quarter-degree box, then the average value of the 5-minute ocean depths in that box was defined to be the depth of the quarter-degree gridbox. If three or more 5-minute squares out of the nine had a common bottom depth, then the depth of the quarter-degree box was set to the most common depth value. The same method was used to go from a quarter-degree to a one-degree resolution. In the one-degree resolution case, at least four points out of a possible sixteen (in a one-degree square) had to be land in order for the one-degree square to remain land and three out of sixteen had to have the same depth for the ocean depth to be set. These criteria yielded a mask that was then modified by :

- a) Connecting the Isthmus of Panama,
- b) maintaining an opening in the Straits of Gibraltar and in the English Channel,
- c) connecting the Kamchatka Peninsula and the Baja Peninsula to their respective continents.

The quarter-degree mask was created as an intermediate step to ensure consistency between the present work and future high resolution analysis of temperature and salinity.

4. RESULTS

4.1 Computation of annual and seasonal fields

After completion of all of our analyses we define a final annual analysis as the average of our twelve monthly mean fields in the upper 500 m of the ocean. Below 500 m depth we define an annual analysis as the mean of the four seasonal analyses. Our final seasonal analyses are defined as the average of monthly analyses in the upper 500 m of the ocean.

4.2 Explanation of standard level figures

All figures showing standard level analyses in this atlas series use similar symbols for displaying information. Continents are indicated as solid - black areas. Ocean areas shallower than the standard depth level being displayed are gray. Gridpoints for which there were less than four one-degree-square values available to correct the first-guess are indicated by an X. Dashed lines represent non-standard contours. "H" and "L" indicate locations of the absolute maximum and minimum of the entire field. All figures were computer drafted.

4.3 Standard level analyses

Global distributions of annual mean nutrients at standard analysis levels are presented in Appendices A, D, and G. Seasonal analyses are presented in Appendices B, E, and H. Seasonal mean minus annual mean difference fields of these variables are also presented in Appendices B, E, and H. Monthly analyses and monthly minus annual mean difference fields are presented in Appendices C, F, and I.

4.4 Contents of the *World Ocean Atlas 2001* CD-ROM

This atlas presents data for selected standard levels in the world oceans. Associated with this atlas, is a CD-ROM containing two parts: digital fields for the world ocean and figures illustrating these data for the world, Pacific, Atlantic and Indian basins. The following is a list of digital fields for the world ocean:

- (a) fields containing the number of observations by one-degree squares as a function of depth;
- (b) one-degree annual objectively analyzed nutrient fields at 33 standard levels (5500 m);
- (c) one-degree seasonal objectively analyzed nutrient fields at 14 standard levels (500 m depth);
- (d) one-degree seasonal minus annual nutrient analyses at 14 standard levels;
- (e) one-degree monthly objective analyses for 14 standard levels;

- (f) one-degree monthly minus annual analyses for 14 standard levels;
- (g) one-degree fields of the annual standard deviation of nutrients at 33 standard depth levels;
- (h) one-degree fields of the seasonal standard deviation of nutrients at 14 standard depth levels;
- (i) one-degree fields of the monthly standard deviation at 14 standard depth levels;
- (j) one-degree fields of the annual standard error of the mean for nutrients at 33 standard depth levels;
- (k) one-degree fields of the seasonal standard error of the mean at 14 standard depth levels;
- (l) one-degree fields of the monthly standard error of the mean at 14 standard depth levels;
- (m) one-degree nutrient unanalyzed annual mean minus objectively analyzed mean values at 33 standard depth levels. These fields represent the combined interpolation and smoothing "error" of our analyses. An example of these statistics is shown in Fig. 4;
- (n) one-degree unanalyzed seasonal mean minus objectively analyzed seasonal mean values at 14 standard levels;
- (o) one-degree unanalyzed monthly mean minus objectively analyzed seasonal mean values at 14 standard levels;
- (p) land-sea file used in the analysis;
- (q) definition of ocean basin masks used in the analysis.

In addition, we present figures of the unanalyzed annual, seasonal, and monthly mean fields (input into the objective analysis) and the number of gridpoints within the influence regions for all standard levels listed above.

The sample standard deviation in a gridbox was computed using:

$$s = \sqrt{\frac{\sum_{n=1}^N (x_n - \bar{x})^2}{N - 1}} \quad (11)$$

in which x_n = the n^{th} data value in the gridbox, \bar{x} = mean of all data values in the gridbox, and N = total number of data values in the gridbox. The standard error of the mean was computed by dividing the standard deviation by the square root of the number of observations in each gridbox.

5. SUMMARY

In the preceding sections we have described the results of a project to objectively analyze all historical nutrient data archived at NODC/WDC, including substantial amounts of data gathered as a result of the NODC and IOC data archaeology and rescue projects. We desire to build a set of climatological analyses that identical in all respects for all variables including relatively data sparse variables such as nutrients. This provides investigators with a consistent set of analyses to work with.

One advantage of the analysis techniques used in this atlas is that we know the amount of smoothing by objective analyses as given by the response function in Table 2 and Figure 2. We believe this to be an important function for constructing and describing a climatology of any geophysical parameter. Particularly when computing anomalies from a standard climatology, it is important that the synoptic field be smoothed to the same extent as the climatology, to prevent generation of spurious anomalies simply through differences in smoothing. A second reason is that purely diagnostic computations require a minimum of seven or eight gridpoints to represent any Fourier component with accuracy. Higher order derivatives will require more smoothing.

We have attempted to create objectively analyzed fields and data sets that can be used as a "black box." We emphasize that some quality control procedures used are subjective. For those users who wish to make their own choices, all the data used in our analyses are available both at standard depth levels as well as observed depth levels (*World Ocean Database 2001* CD-ROM set - Conkright *et al.*, 2002b). The results presented in this atlas show some features that are suspect and may be due to nonrepresentative or incorrect data that were not flagged by the quality control techniques used. Although we have attempted to eliminate as many of these features as possible by flagging the data which generate these features some obviously remain. Some may eventually turn out not to be artifacts but rather to represent real features, not yet capable of being described in a meaningful way due to lack of data.

6. FUTURE WORK

Our analyses will be updated when justified by additional observations. As more data are received at NODC/WDC, we will also be able to produce higher resolution climatologies for each variable as Boyer and Levitus (1997) have done for temperature and salinity.

References

- Achtemeier, G. L., 1987: On the concept of varying influence radii for a successive corrections objective analysis. *Monthly Weather Review*, 11, 1761-1771.
- Barnes, S. L., 1964: A technique for maximizing details in numerical weather map analysis. *J. App. Meteor.*, 3, 396-409.
- _____ 1973: Mesoscale objective map analysis using weighted time series observations. *NOAA Technical Memorandum ERL NSSL-62*, 60 pp.
- _____ 1994: Applications of the Barnes Objective Analysis Scheme, Part III: Tuning for Minimum Error. *J. Atmosph. and Oceanic Tech.* 11:1459-1479.
- Bergthorsson, P., and B. Doos, 1955: Numerical Weather map analysis. *Tellus*, 7, 329-340.
- Boyer, T.P., and S. Levitus, 1997: *Objective Analyses of temperature and salinity for the world ocean on a 1/4 ° grid. NOAA/NESDIS Atlas 11*. U.S. Gov. Printing Office, Wash., D.C., 62 pp.
- Conkright, M. E., Levitus, S., and Boyer, T. P., 1994a: *World Ocean Atlas 1994, Vol 1: Nutrients*. National Oceanic and Atmospheric Administration, Wash., D.C., 150 pp.
- Conkright, M.E., Boyer, T. P., and S. Levitus, 1994b: Quality control and processing of historical oceanographic nutrient data. *NOAA Technical Report NESDIS 79*, 75 pp.
- Conkright, M., T. O'Brien, S. Levitus, T.P. Boyer, 1998: World Ocean Atlas 1998 Vol. 1: Atlantic Ocean nutrient and chlorophyll fields. *U.S. Gov. Printing Office, Wash., D.C.*, 245 pp.
- Conkright, M.E., J.I. Antonov, O. Baranova, T. P. Boyer, H.E. Garcia, R. Gelfeld, D. Johnson, R.A. Locarnini, P.P. Murphy, T.D. O'Brien, I. Smolyar, C. Stephens, 2002a: *World Ocean Database 2001, Volume 1: Introduction*. S. Levitus, Ed., NOAA Atlas NESDIS 42, U.S. Government Printing Office, Washington, D.C., 167 pp., CD-ROMs.
- Conkright, M. E., T. O'Brien, T.P. Boyer, C. Stephens, R. A. Locarnini, H. E. Garcia, P. P. Murphy, D. Johnson, O. Baranova, J. I. Antonov, R. Tatusko, R. Gelfeld, I. Smolyar, 2002b: *World Ocean Database 2001 CD-ROM Data Set Documentation*. National Oceanographic Data Center, Silver Spring, MD, 137 pp.
- Cressman, G. P., 1959: An operational objective analysis scheme. *Mon. Wea. Rev.*, 87, 329-340.
- Daley, R., 1991: *Atmospheric Data Analysis*. Cambridge University Press, Cambridge, 457 pp.
- England, M.H., 1992: On the formation of Antarctic Intermediate and Bottom Water in Ocean general circulation models. *J. Phys. Oceanogr.*, 22, 918- 926.
- ETOPO5, 1988: Data Announcements 88-MGG-02, Digital relief of the Surface of the Earth. NOAA, National Geophysical Data Center, Boulder, CO.
- Gandin, L.S., 1963: *Objective Analysis of Meteorological fields*. Gidrometeorol Izdat, Leningrad (translation by Israel program for Scientific Translations, Jerusalem, 1966); 242 pp.
- IPCC, Intergovernmental Panel on Climate Change, 1996: *Climate Change 1995 - The Science of Climate Change, Contribution of Working Group I to the Second Assessment Report of the Intergovernmental Panel on Climate Change*. Editors J.J. Houghton, L.G. Meiro Filho, B.A. Callander, N. Harris, A. Kattenberg, and K. Maskell. Cambridge University Press, Cambridge, UK, 572 pp.
- JPOTS (Joint Panel on Oceanographic Tables and Standards) Editorial Panel, 1991: Processing of Oceanographic Station Data. UNESCO, Paris, 138 pp.
- Levitus, S., 1982: *Climatological Atlas of the World Ocean*, NOAA Professional Paper No. 13, U.S. Gov. Printing Office, 173 pp.

- Rabiner, L. R., M. R. Sambur, and C. E. Schmidt, 1975: *Applications of a nonlinear smoothing algorithm to speech processing, IEEE Trans. on Acoustics, Speech and Signal Processing*, Vol. Assp-23, 552-557.
- Reiniger, R.F., and C.F. Ross, 1968: A method of interpolation with application to oceanographic data. *Deep-Sea Res.*, 9, 185-193.
- Sasaki, Y., 1960: An objective analysis for determining initial conditions for the primitive equations. Ref. 60-1 6T, Atmospheric Research Lab., Univ. of Oklahoma Research Institute, Norman, 23 pp.
- Seaman, R. S., 1983. Objective Analysis accuracies of statistical interpolation and successive correction schemes. *Australian Meteor. Mag.*, 31, 225-240.
- Shuman, F. G., 1957: Numerical methods in weather prediction: II. Smoothing and filtering. *Mon. Wea. Rev.*, 85, 357-361.
- Smith, D. R., and F. Leslie, 1984: Error determination of a successive correction type objective analysis scheme. *J. Atm. and Oceanic Tech.*, 1, 121-130.
- Smith, D.R., M.E. Pumphry, and J.T. Snow, 1986: A comparison of errors in objectively analyzed fields for uniform and nonuniform station distribution, *J. Atm. Oceanic Tech.*, 3, 84-97.
- Sverdrup, H.U., M.W. Johnson, and R.H. Fleming, 1942: *The Oceans: Their physics, chemistry, and general biology*. Prentice Hall, 1060 pp.
- Thiebaux, H.J., M.A. Pedder, 1987: *Spatial Objective Analysis: with applications in atmospheric science*. Academic Press, 299 pp.
- Tukey, J. W., 1974: Nonlinear (nonsuperposable) methods for smoothing data, in "*Cong. Rec.*", 1974 EASCON, 673 pp.

Table 1. Acceptable distances (m) for defining interior and exterior values used in the Reiniger-Ross scheme for interpolating observed level data to standard levels.

Standard Level number	Standard depths (m)	Acceptable distances (m) for interior values	Acceptable distances (m) for exterior values
1	0	5	200
2	10	50	200
3	20	50	200
4	30	50	200
5	50	50	200
6	75	50	200
7	100	50	200
8	125	50	200
9	150	50	200
10	200	50	200
11	250	100	200
12	300	100	200
13	400	100	200
14	500	100	400
15	600	100	400
16	700	100	400
17	800	100	400
18	900	200	400
19	1000	200	400
20	1100	200	400
21	1200	200	400
22	1300	200	1000
23	1400	200	1000
24	1500	200	1000
25	1750	200	1000
26	2000	1000	1000
27	2500	1000	1000
28	3000	1000	1000
29	3500	1000	1000
30	4000	1000	1000
31	4500	1000	1000
32	5000	1000	1000
33	5500	1000	1000

Table 2. Response function of the objective analysis scheme as a function of wavelength for WOA01 and earlier analyses.

Wavelength*	Levitus (1982)	WOA94	WOA98 - WOA01
360ΔX	1.000	0.999	1.000
180ΔX	1.000	0.997	0.999
120ΔX	1.000	0.994	0.999
90ΔX	1.000	0.989	0.998
72ΔX	1.000	0.983	0.997
60ΔX	1.000	0.976	0.995
45ΔX	1.000	0.957	0.992
40ΔX	0.999	0.946	0.990
36ΔX	0.999	0.934	0.987
30ΔX	0.996	0.907	0.981
24ΔX	0.983	0.857	0.969
20ΔX	0.955	0.801	0.952
18ΔX	0.923	0.759	0.937
15ΔX	0.828	0.671	0.898
12ΔX	0.626	0.532	0.813
10ΔX	0.417	0.397	0.698
9ΔX	0.299	0.315	0.611
8ΔX	0.186	0.226	0.500
6ΔX	3.75×10^{-2}	0.059	0.229
5ΔX	1.34×10^{-2}	0.019	0.105
4ΔX	1.32×10^{-3}	2.23×10^{-3}	2.75×10^{-2}
3ΔX	2.51×10^{-3}	1.90×10^{-4}	5.41×10^{-3}
2ΔX	5.61×10^{-7}	5.30×10^{-7}	1.36×10^{-6}

* For ΔX = 111 km

Table 3. Basins defined for objective analysis and the shallowest standard depth level for which each basin is defined.

BASIN	STANDARD DEPTH	BASIN	STANDARD DEPTH
Aleutian Basin	28	Gulf of Mexico	26
Andaman Basin	25	Hudson Bay	1
Arabian Sea	30	Indian Ocean	1 *
Arctic Ocean	1 *	Java Sea	6
Argentine Basin	31	Kara Sea	8
Atlantic Indian Basin	31	Marianas Basin	30
Atlantic Ocean	1 *	Mascarene Basin	30
Baffin Bay	14	Mediterranean Sea	1 *
Baltic Sea	1	North Caribbean	26
Banda Sea	23	North American Basin	29
Barents Sea	28	Pacific Ocean	1 *
Bay of Bengal	1 *	Persian Gulf	1
Beaufort Sea	28	Philippine Sea	30
Black Sea	1	Red Sea	1
Brazil Basin	31	Sea of Okhotsk	19
Caribbean Sea	23	Sea of Japan	1
Caspian Sea	1	Somali Basin	30
Celebes Sea	25	South China Sea	28
Central Indian Basin	29	Southeast Pacific Basin	29
Chile Basin	30	Southeast Indian Basin	29
Coral Sea	29	Southeast Atlantic Basin	29
Crosat Basin	30	Southern Ocean	1 *
East Atlantic Indian Basin	32	Southwest Atlantic Basin	29
East Indian Basin	29	Sulu Sea	10
East Mediterranean	16	Sulu Sea II	14
East Caroline Basin	30	Tasman Sea	30
Fiji Basin	29	Venezuela Basin	14
Guatemala Basin	29	West Mediterranean	19
Guinea Basin	30	West European Basin	29

Basins marked with a “” can interact with adjacent basins

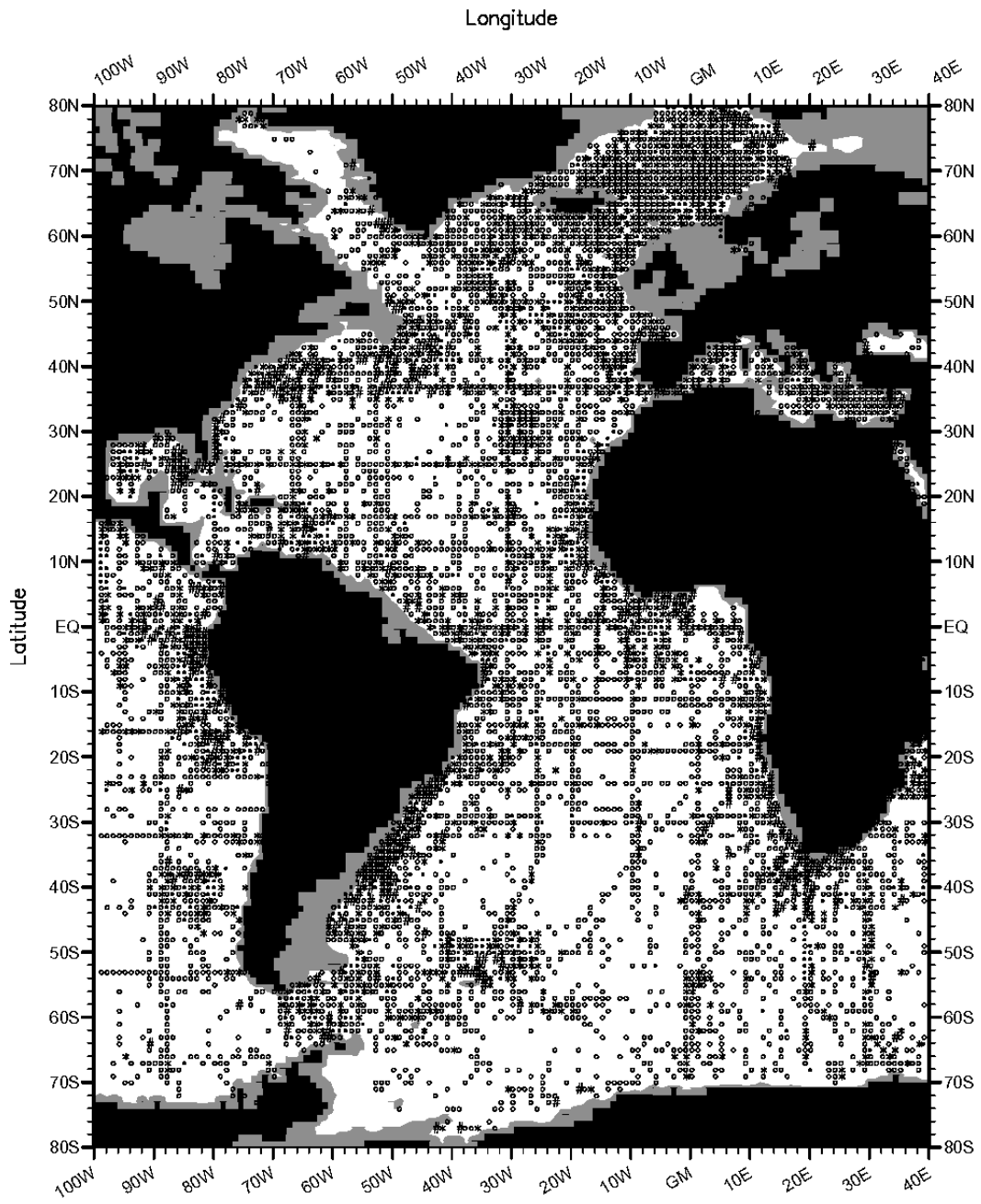


Fig. 1a. Annual phosphate standard deviation (μM) at 500 meters depth by one-degree squares

$\leq 0.05 = \circ$ $0.05 - 0.15 = *$ $0.15 - 0.25 = \bullet$ $> 0.25 = \#$

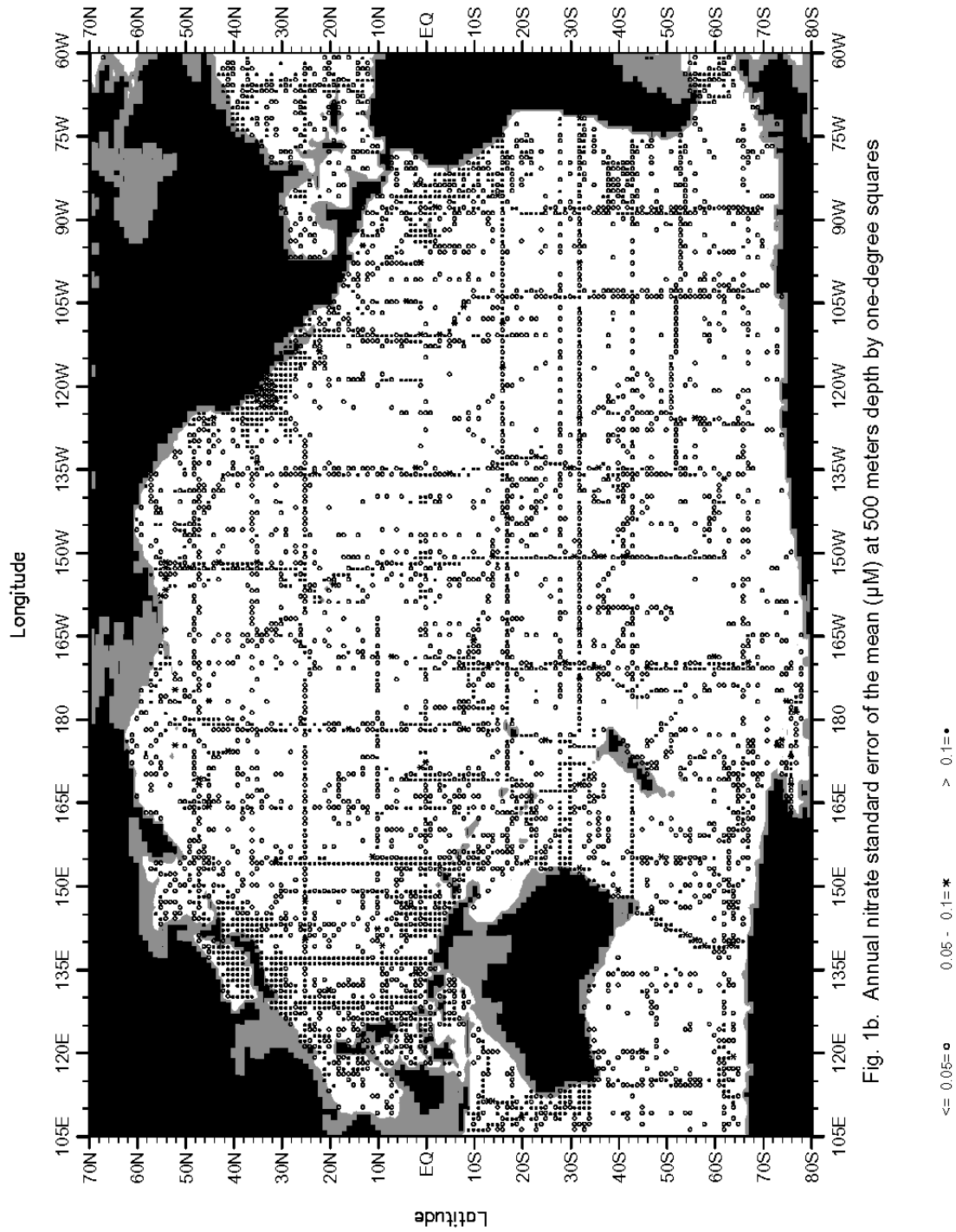


Fig. 1b. Annual nitrate standard error of the mean (μM) at 500 meters depth by one-degree squares

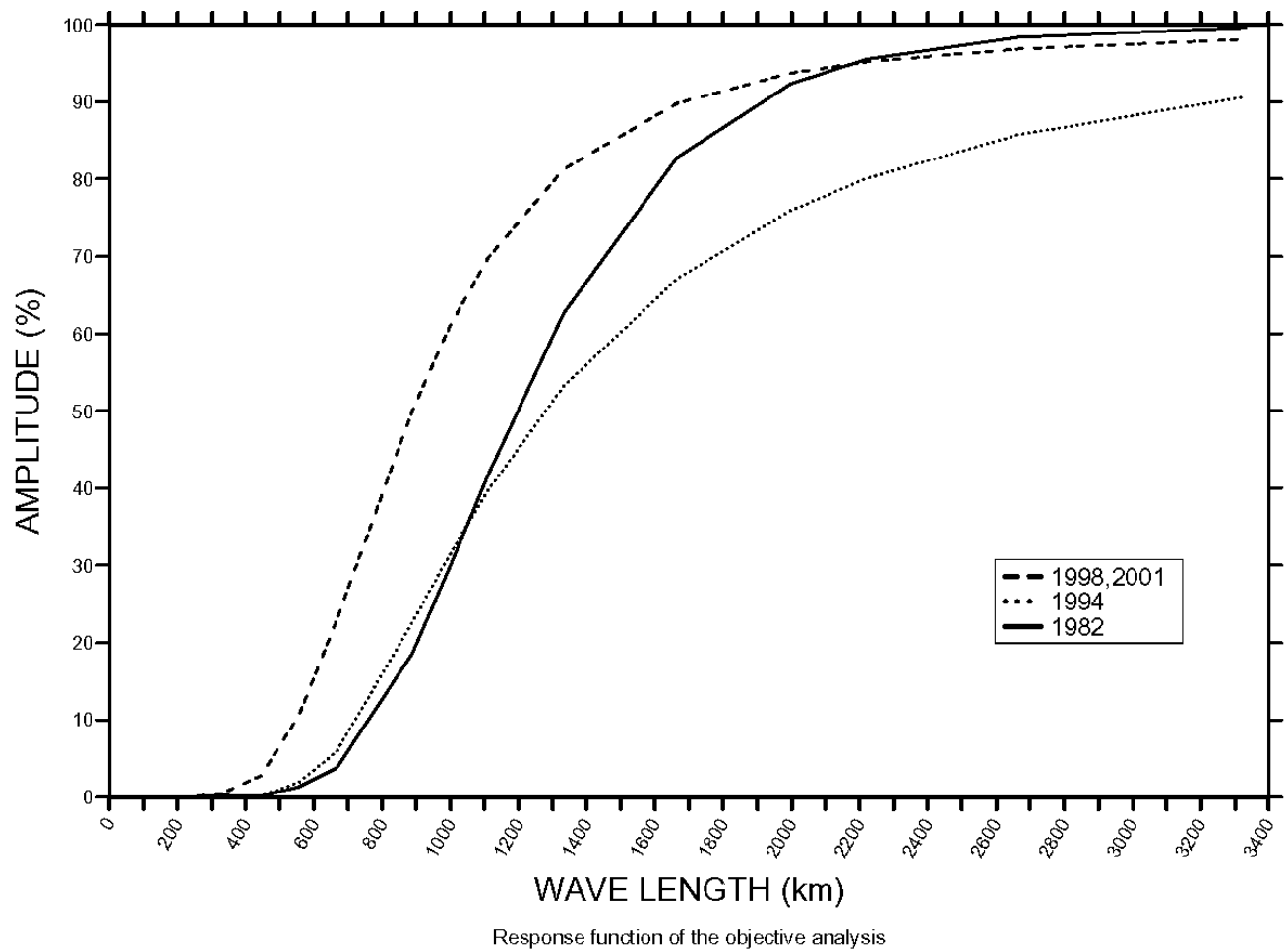


Figure 2. Response function of the WOA01, WOA98, WOA94, and Levitus (1982) objective analysis schemes.

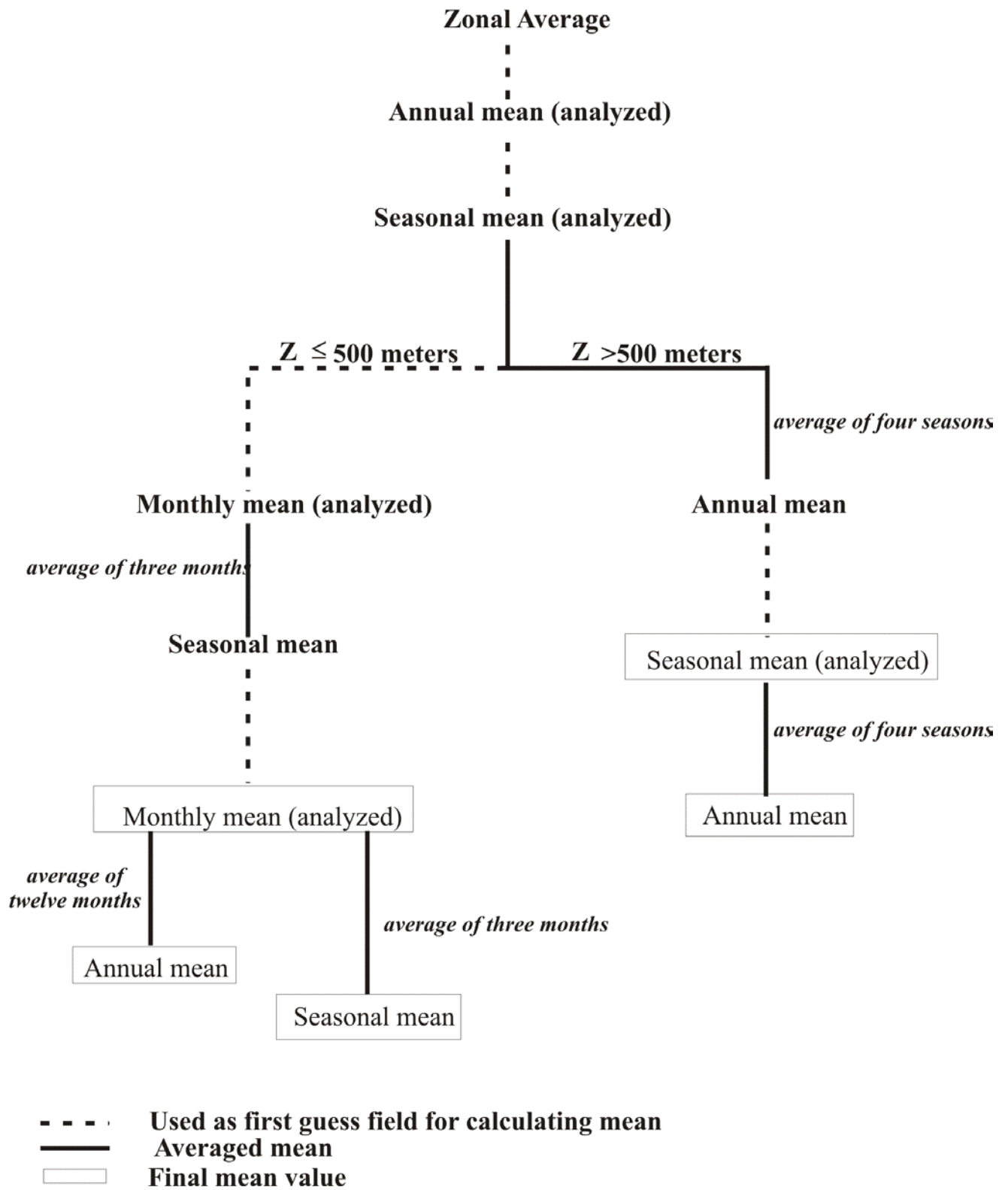


Figure 3. Scheme used in computing annual, seasonal, and monthly objectively analyzed means for a variable.

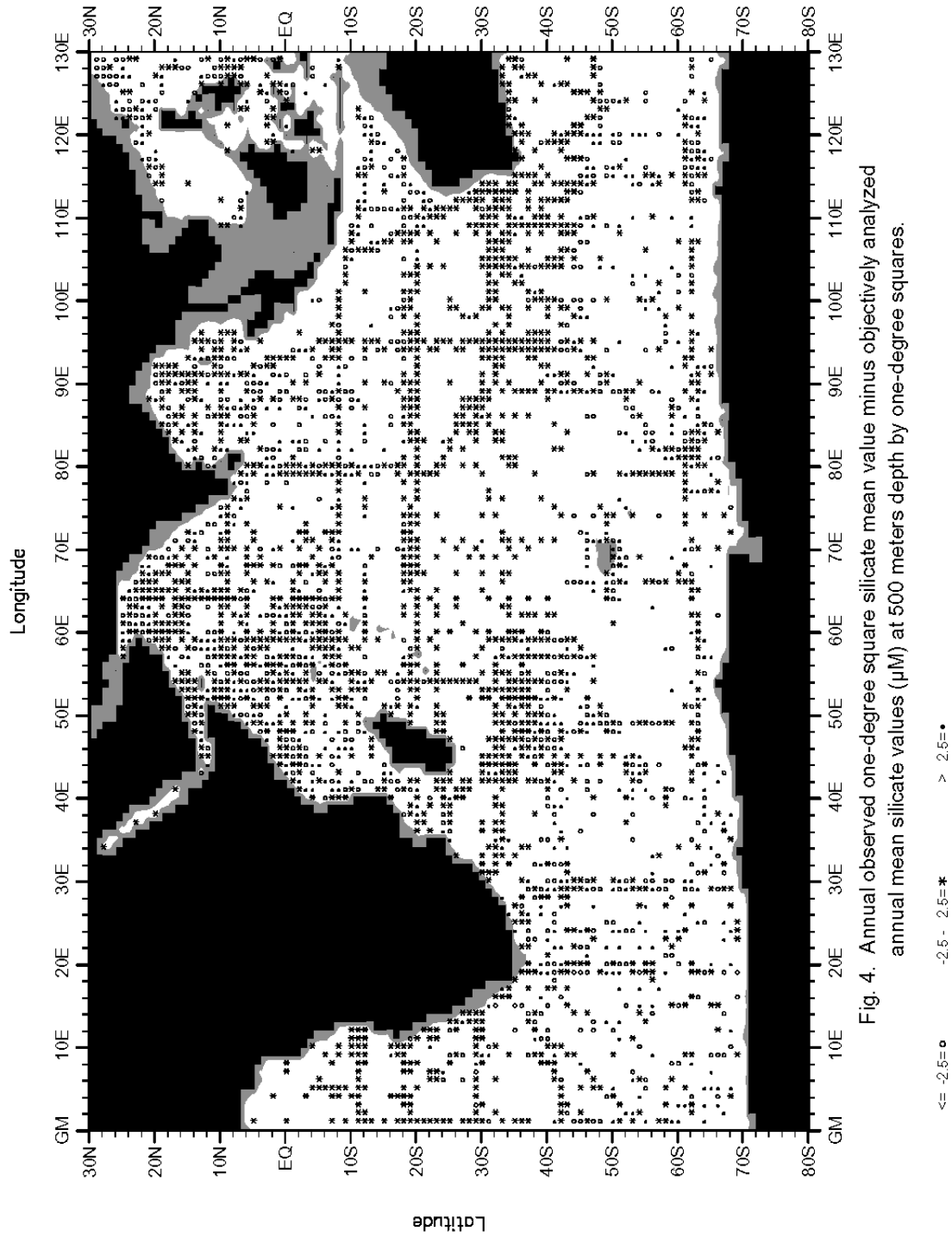


Fig. 4. Annual observed one-degree square silicate mean value minus objectively analyzed annual mean silicate values (μM) at 500 meters depth by one-degree squares.

APPENDICES

In each data distribution figure in each appendix, a small dot indicates a one-degree square containing 1-4 observations and a large dot indicates a one-degree square containing five or more observations.

In each figure showing an objectively analyzed mean field or difference between seasonal (monthly) mean and annual mean, gridpoints for which there were less than four one-degree square values available to correct the first-guess are indicated by an “x”.